

Characterization of Dusty Debris Disks: the IRAS and Hipparcos Catalogs

Joseph H. Rhee¹, Inseok Song¹ B. Zuckerman², and Michael McElwain²

Received _____; accepted _____

To appear in ApJ, 2006

¹Gemini Observatory, 670 North A'ohoku Place, Hilo, HI 96720; jrhee@gemini.edu, song@gemini.edu

²Department of Physics and Astronomy and NASA Astrobiology Institute UCLA, Los Angeles, CA 90095; ben@astro.ucla.edu, mcelwain@astro.ucla.edu

ABSTRACT

Dusty debris disks around main sequence stars are signposts for the existence of planetesimals and exoplanets. From cross-correlating Hipparcos stars with the IRAS catalogs, we identify 153 stars within 120 pc of Earth that show excess emission at 60 μ m. This search took special precautions to avoid false positives. Our sample is reasonably well distributed from late B to early K type stars, but it contains very few later type stars. Even though IRAS flew more than 20 years ago and many astronomers have cross correlated its catalogs with stellar catalogs, we were still able to newly identify debris disks at 37 main sequence stars; of these, 35 are within 100 pc of Earth. The power of an all-sky survey satellite like IRAS is evident when comparing our 37 new debris disks with the total of only 22 dusty debris disk stars first detected with the more sensitive, but pointed, satellite ISO. Our findings indicate: (1) as one progresses from stellar ages of \sim 10 Myr to a few Gyr, a smaller percentage of stars display fractional infrared luminosities τ ($= L_{IR}/L_{bol}$) above the IRAS threshold which is about 10^{-5} . (2) Peak τ is a few times 10^{-3} at all ages later than \sim 10 Myr; this might be because occasional catastrophic dust-generating events can occur at any age. (3) The spread of measured τ at ages \sim 10 Myr is about a factor of 10, increasing to about 100 at later ages; given the measured peak τ (item 2) and IRAS threshold (item 1), the measured spread of τ cannot be greater than 100. (4) At any given age late-type stars tend to have the largest τ s. (5) For early-type stars between \sim 10 and 100 Myr of age, the typical radius of a dusty debris disk appears to be smaller than for stars with ages between 100 Myr and 1 Gyr. (6) The very largest τ s ($> 10^{-3}$) are associated only with disks that have relatively small radii. (7) The ratio of τ to disk mass deduced from submillimeter photometry varies approximately as the inverse square of dust orbital semimajor axis, as expected for optically thin

disks containing particles of similar sizes and densities. (8) For 61 stars with ages > 10 Myr and dust disk radius < 100 AU, dust masses estimated from far-IR emission detected by IRAS lie between 0.0005 and $0.5 M_{\oplus}$. (9) Our technique for deriving disk dust masses solely from far-IR emission data can be applied directly to main sequence stars with excess emission detected by *Spitzer* at two or more well separated wavelengths; i.e., dust mass estimates at such stars need not await submillimeter photometry measurements. (10) Two early-type stars in the ~ 600 Myr old Hyades are found to have excess $60 \mu\text{m}$ emission, implying a debris disk fraction of 5% with IRAS sensitivity (τ a few times 10^{-5}) at this age and distance from Earth. (11) IRAS detected excess $60 \mu\text{m}$ emission from $\sim 20\%$ of nearby A-type stars. (12) Four Algol-type eclipsing binaries, including Algol A itself, display $60 \mu\text{m}$ emission, generated by free-free and bound-free transitions in ionized gas or by dust grains or by both. (13) GL 803 (AU Mic, 12 Myr old) is the only M-type, non-T Tauri, Hipparcos dwarf star to display $60 \mu\text{m}$ excess emission in the IRAS Catalogs.

Subject headings: Infrared Excess, Young stars

1. Introduction

Dusty debris disks that surround nearby main sequence stars were first detected by the Infrared Astronomical Satellite (IRAS) in 1983. These circumstellar disks were inferred from an infrared excess flux between 25 and $100 \mu\text{m}$ many times brighter than expected from the stellar photosphere. The IR excess was modeled by disk distributions that would absorb optical and ultraviolet flux from the host star and then isotropically radiate this energy at infrared. The first dusty debris disk was discovered around the bright main sequence star Vega (Aumann et al. 1984), consequently the dusty disk characteristic at

main sequence stars is commonly referred to as the Vega phenomenon.

Numerous studies of T Tauri stars dating back many years indicate the characteristic time scale for the dispersal of a surrounding dusty, gaseous disk is a few Myr. Following dissipation of the gaseous component, remaining dust can further dissipate during the following few million years via coagulation into large objects, Poynting-Robertson and stellar wind drag, radiation pressure, and collisional destruction (e.g., Backman & Paresce 1993; Lagrange, Backman, & Artymowicz 2000; Dominik & Decin 2003; Plavchan et al. 2005). Vega-like stars are, however, generally much older than 10 Myr, thus the observed dust should be of secondary origin, most likely replenished via collision and fragmentation of planetesimals. Furthermore, the Vega-phenomenon overlaps with the important planetary system formation epochs in our Solar System: giant gas planet formation within \sim 10 Myr, terrestrial planet formation within \sim 30 Myr, and the era of heavy bombardment in the inner Solar System within \sim 600 Myr. Therefore, studies of IR excess stars can provide crucial information on extrasolar planetary formation and evolution.

During the past two decades, about two dozen papers have been published that describe IRAS, ISO (Infrared Space Observatory), and *Spitzer Space Telescope* searches for stars with excess IR emission (§ 3; Lagrange, Backman, & Artymowicz 2000; Zuckerman 2001; Decin et al. 2003). These searches employed different techniques for cross-correlating IR and stellar sources with no consistent definition of an IR excess. To date, several hundred main sequence infrared excess stars have been reported in the literature including those that have IR excess at $25\ \mu\text{m}$. However, a significant percentage of suggested IR excess stars might be misidentifications due to the large beam size of IRAS and improper search or calibration techniques. Such contamination of the debris disk population has not only plagued many follow-up observations from ground and/or space observatories but also precludes a global assessment of the distribution and evolution of the dust population.

A major goal of debris disk research has been to characterize the temporal evolution of the quantity of dust present in the disks. Notwithstanding almost two decades of debris disk research utilizing data from three infrared satellites, a convincing assessment of this temporal evolution remains incomplete. Such an assessment requires a large sample of stars and a reliable estimate of the dust mass and the age for each debris disk system. False positive IR excess stars have contaminated determination of the amount of dust in some previous studies, thus confusing results from the beginning. If the IR excess is from a bona fide dust disk, then the best estimator of dust mass comes from submillimeter flux. Unfortunately, submillimeter flux measurements are difficult, time intensive observations. A more readily accessible observable is τ , the ratio of excess infrared luminosity due to dust divided by the total energy output from a star. We compute values of τ for each of the IR excess stars presented in this paper. In § 5.1 we discuss the relationship between submillimeter flux and τ for those Vega-like stars where both are known, and we derive our own relationship which is used to predict a dust mass if both τ and the dust disk radius are known.

Furthermore, estimation of stellar age is often troublesome since most nearby IR excess stars are isolated field stars. In order to obviate the shortcoming of stellar age estimation, several groups are using *Spitzer* to search for IR excess stars in nearby young stellar groups with well-determined ages (e.g., Stauffer et al. 2005). However, because the distance to all rich clusters is substantial (except for the Hyades), it remains difficult to obtain statistically significant results even with *Spitzer* (Stauffer et al. 2005). Thus, the large, clean sample of relatively nearby field stars we discuss in the present paper can contribute in a statistically meaningful way to our understanding of the Vega phenomenon and its evolution with time.

2. Search Criteria and Selection Technique

Zuckerman & Song (2004a) (hereafter Paper I), relying primarily on data in Silverstone's (2000) thesis, analyzed 58 strong excess stars following careful checks against possible contamination from various sources. Zuckerman & Song argued that the Vega-like stars are signposts for the existence of planets and focused their efforts on identifying stars that would make the best targets for adaptive optics and precision radial velocity searches. The present paper extends the sample analyzed in Paper I in a couple of ways. First, we significantly increase the sample size so that it is now possible to address circumstellar dusty disk evolution in a statistically meaningful way. This increase is achieved by systematically cross-correlating all Hipparcos main-sequence stars with $60\ \mu\text{m}$ IRAS sources in the Faint Source (FSC) and Point Source (PSC) catalogs. Our distance limit is 120 pc compared with the 100 pc adopted in Paper I. Second, the Spectral Energy Distribution (SED) fitting routine was enhanced with the employment of filter response functions and a fully automated fit with χ^2 minimization method.

Hipparcos, 2MASS, and IRAS data were cross-correlated to search for IR excess stars. Many sources in the FSC and PSC with optical stellar identifications are, however, giant stars (Odenwald 1986; Zuckerman et al. 1995a). A constraint on the absolute visual magnitude $M_V \geq 6.0(B-V) - 2.0$ (Figure 1) was applied to the entire 118,218 stars of the Hipparcos catalog to remove giant stars from our sample. This cut eliminated 50,164 stars, leaving 68,054 Hipparcos stars for further investigation.

Then, these pre-screened Hipparcos dwarfs were cross-correlated against IRAS sources. The IRAS FSC was used to cross-correlate the 53,157 stars located out of the Galactic plane ($|b| > 10^\circ$), while the PSC was used for the 14,897 stars in the Galactic plane and to recover any object missed by the FSC out of the Galactic plane. All FSC sources with a detection at $60\ \mu\text{m}$ (i.e. a $60\ \mu\text{m}$ flux quality of 2 or 3) and a Hipparcos dwarf within

$45''$ were selected for further investigation. A search radius of $45''$ was adopted to reflect the average FSC 3σ positional error. For PSC sources in the Galactic plane, Hipparcos dwarfs within only a $10''$ search radius were retained, in order to avoid contamination of spurious sources in the crowded fields of the Galactic plane. There were 557 stars (481 from the FSC and 76 from the PSC) that passed the initial cross-correlation. Unfortunately, the FSC is only $\sim 80\%$ complete. We therefore cross-correlated all main sequence Hipparcos stars outside the Galactic plane with the PSC using a search radius of $45''$. We found an additional 65 stars in the PSC that had $60\text{ }\mu\text{m}$ detections, but were unidentified in the FSC. Most of these stars from the PSC were detected at $12\text{ }\mu\text{m}$ (but not $60\text{ }\mu\text{m}$) in the FSC. In contrast, Silverstone (2000) cross-correlated Hipparcos and IRAS FSC sources only. Our correlation with the IRAS FSC and PSC left a collection of 622 main sequence stars identified in the Hipparcos catalog which had $60\text{ }\mu\text{m}$ counterparts detected by IRAS.

In young and massive main sequence stars, significant IR flux arises from free-free emission. Such stars, namely spectral types O1 thru B5, were excluded from our sample by rejection of objects whose $B - V$ is more negative than -0.15. In calculating $B - V$, we converted Tycho B and V magnitudes into Johnson B and V magnitudes following the description given in Bessell (2000). Then a distance cut of 120 pc was applied to our sample to avoid contaminations arising from star-forming regions and interstellar cirrus as described, for example, in Kalas et al. (2002) (see below).

A visual inspection of the remaining excess candidates for the presence of a background galaxy was conducted by correlating the FSC and PSC catalogs with NASA's Extragalactic Database (NED) in Digital Sky Survey (DSS) images. Any star with a noticeable galaxy within the 3σ IRAS positional error ellipse was removed from our sample, and any star with a bright star within the 3σ error ellipse was flagged for further checking of its SED. Since NED is not complete, we also carefully checked any DSS optical extended sources (mainly

galaxies) which were not included in NED. Using the long format of the FSC catalog, Silverstone (2000) compared the 60 μm position to the stellar position and excluded stars whose 60 μm offsets are $> 30''$. Instead of imposing such a strict constraint on our sample, we exclude stars only if their 60 μm offsets are greater than the 3σ IRAS positional error. For all FSC sources, we carefully checked their 60 μm positions against any galaxy or bright nearby star.

For stars with apparent detections in the IRAS 100 μm band, we tested for possible contamination from interstellar cirrus. Some relatively distant, previously known, IR excess candidates are contaminated by interstellar cirrus (Kalas et al. 2002). We checked the IRAS cirrus flag of all 100 μm sources and rejected those with cirrus flag > 3 except HIP 77542. HIP 77542 had significant excess at all wavelengths and was fit nicely with a single blackbody temperature (Paper I).

A fully automated spectral energy distribution (SED) fit technique using a theoretical atmospheric model (Hauschildt, et al. 1999) was used to predict stellar photospheric fluxes. This fit technique is unlike previous excess searches which use the “empirical” color of main sequence stars to estimate stellar photospheric fluxes. For each star, fluxes at five standard Johnson bands (B , V , J , H , and K) were employed to fit the model spectra of a stellar photosphere. The standard B and V magnitudes were obtained by converting Tycho B and V magnitudes using values interpolated from Table 2 in Bessell (2000). For the ten Hipparcos objects that did not have observed Tycho B and V magnitudes, B and V values were obtained from SIMBAD. Observed J , H , and K_s magnitudes came from the 2MASS catalog. When any star was brighter than 5th magnitude at J , H , or K_s in 2MASS, we set its uncertainty to 0.400 mag. The zero magnitudes in Cox (2000) were used to convert the observed magnitudes into a flux density (Jy). The current Hauschildt et al. stellar photosphere model (T. Barman, private communication) is available for effective

temperatures from 1700 K to 10,000 K (in 100 K increments from 1700 K to 3000 K and in 200 K increments from 3000 K to 10,000 K). The stellar radius and effective temperature were used as free parameters to fit the observed fluxes with a χ^2 minimization method.

We created model fluxes at each band by convolving each filter function with the model spectra. This method provides a more accurate representation of the observed flux especially where the passband includes significant spectral features such as the Balmer jump. Comparing the best-fit model spectra with the observed fluxes, we found that the model spectra always overestimated the V -band flux. This perhaps arises from some missing opacity sources in the V -band of the model spectra. For consistency, we manually set the uncertainty of a V -band magnitude to 0.25 if the given uncertainty value is smaller than 0.25 mag to ensure a better fit.

Once the stellar photosphere was modeled, a dust component was fit with a blackbody curve. IRAS upper limits were not included in the dust fitting, but we mandated that the upper limits are always above the estimated total (star & dust) flux. Temperature dependent IRAS color corrections should be carefully considered. Both the stellar photosphere and dust emission contribute to the observed IRAS flux as follows,

$$F_{IRAS}^{observed} = F_{photosphere}^{uncorrected} + F_{dust}^{uncorrected} \quad (1)$$

Thus accurate estimation of a color correction value requires not only the flux of the stellar photosphere but also that of dust which is obtained through the blackbody fitting. But the problem is that both dust flux and the color correction are a function of dust temperature, which requires an iterative process to determine the dust temperature in color-corrected IRAS dust flux. Instead we obtained the dust temperature by fitting the uncorrected IRAS fluxes. First, we “COLORED” the stellar photosphere (Eq. 2) by multiplying the appropriate color correction terms (K_{star}) before subtracting the stellar

photosphere (Eq. 3).

$$F_{\text{photosphere}}^{\text{uncorrected}} = F_{\text{photosphere, model}} \times K_{\text{star}} \quad (2)$$

$$F_{\text{dust, model}}^{\text{uncorrected}} = F_{\text{IRAS}}^{\text{observed}} - F_{\text{photosphere, model}} \times K_{\text{star}} \quad (3)$$

Then we fit the remaining IRAS fluxes with the “COLORED” blackbody curve (Eq. 4).

$$F_{\text{dust, model}}^{\text{uncorrected}} = F_{\text{dust, model}} \times K_{\text{dust}} \quad (4)$$

By combining Eq. 3 & 4 and using the stellar photosphere model described above, we obtained the best fit temperatures of the stellar and dust emission. Then the correct total IRAS color correction terms were calculated by estimating the fractional color terms using a weighted average of photosphere and dust fluxes at each wavelength (Eq. 5).

$$K_{\text{total}} = C_1 \times K_{\text{star}}^{\text{bestfit}} + C_2 \times K_{\text{dust}}^{\text{bestfit}} \quad (5)$$

where C_1 and C_2 are the fractional contributions of the stellar photosphere and dust to the total measured flux.

$$F_{\text{IRAS}}^{\text{true}} = F_{\text{IRAS}}^{\text{observed}} / K_{\text{total}} \quad (6)$$

In displaying the IRAS observed magnitudes, we applied the prorated color correction terms to the IRAS measurements (Eq. 6). As in photosphere fitting, we created synthetic fluxes at each IRAS band by convolving IRAS filter functions with the blackbody curve.

SED fits were performed for all identified IRAS and Hipparcos stars, yielding very precise estimation of stellar photospheric fluxes (Figure 2). When available, additional

fluxes from ISO³ and/or *Spitzer*⁴ measurements were used to better fit dust components. Five objects were dropped from our list due to possible cirrus contamination or no 60 μm excess based on ISO measurements reported in Silverstone (2000). For some objects, *Spitzer* MIPS data are available in the public archive but were not published. In such cases, we extracted photometry from MIPS pipeline data at 24 and 70 μm . No photometry was attempted on MIPS 160 μm pipeline data because of heavy contamination from a known “blue leak”.

Several class I & II pre-main sequence (PMS) stars were found from our SED fits, where a typical SED of a class I/II PMS star shows large B and V fluxes above the model spectrum and strong but flat excess in the IR. Because we are searching for IR excess among main-sequence stars, class I & II PMS stars were subsequently eliminated from our sample. For completeness, the IRAS-identified Hipparcos class I & II PMS stars within 120 pc are listed in Table 1.

Many sources that passed the visual check, especially nearby stars, showed no IR excess in their SED. Color corrected IRAS fluxes were compared to the estimated photospheric fluxes. Stars with no IR excess ($[\text{F}_{\text{IRAS}} - \text{F}_{\text{photosphere}}] / \sigma_{\text{IRAS}} < 2.5$) were eliminated except HIP 71284. IR excess in HIP 71284 was confirmed by an ISO observation (Paper I). 149 stars had IR excess ($[\text{F}_{\text{IRAS}} - \text{F}_{\text{photosphere}}] / \sigma_{\text{IRAS}} > 3.0$), and eight stars showed marginal IR excess ($2.5 < [\text{F}_{\text{IRAS}} - \text{F}_{\text{photosphere}}] / \sigma_{\text{IRAS}} < 3.0$). These marginal IR excess stars fall into a statistical domain in which $\sim 0.5\%$ of non-excess stars may produce a false excess assuming Gaussian noise. For this study, more than 600 Hipparcos dwarfs within 120 pc with IRAS 60 μm detection may yield 3 or 4 false excess stars. Recent *Spitzer* observations show that 3 stars (HIP 28103, HIP 105090, & HIP 105858) that had marginal IR excess

³ISO measurements were taken from Silverstone (2000) and Habing et al. (2001).

⁴*Spitzer* MIPS measurements were taken from the references given in § 3.

from IRAS are not, in fact, IR excess stars.

After dropping those three stars but including HIP 71284, we finally present 153 IRAS identified Hipparcos IR excess dwarfs in this paper. Among them 37 stars are newly identified as IR excess stars from our survey, and only two objects out of these 37 newly identified IR excess stars have marginal IR excess ($2.5 < [F_{IRAS} - F_{photosphere}] / \sigma_{IRAS} < 3.0$).

3. Overview of previous IRAS, ISO and *Spitzer* surveys for dusty debris disks

Comparison of IRAS with ISO and *Spitzer* demonstrates the power of all-sky surveys. Notwithstanding that IRAS flew more than 20 years ago, through careful analysis of its database, we have been able to discover 37 main-sequence Hipparcos stars with previously unrecognized dusty debris disks detected at $60 \mu\text{m}$ wavelength. In comparison, only 22 new $60 \mu\text{m}$ excess stars were discovered in all ISO programs while ~ 20 new $70 \mu\text{m}$ excess stars were announced in the 2004 and 2005 *Spitzer*-based literature (see below for references). Although ISO and *Spitzer* have higher sensitivities than IRAS, they are both pointed satellites with a much smaller sky coverage.

IRAS surveys and, significantly, some of their limitations are summarized in § 1 of the present paper and in § 3 of Zuckerman (2001). Previous to the present study, Murray Silverstone's Ph.D. thesis (2000) represented the most comprehensive search of the IRAS catalogs for Vega-like $60 \mu\text{m}$ excess stars. However, Silverstone's primary goal was to use ISO to detect dust at F- and G-type stars inconclusively detected by IRAS at $60 \mu\text{m}$. He did not analyze his IRAS findings, and his search never reached publication. Thus, no IRAS survey published prior to 2006 is germane to issues addressed in the present paper.

ISO was a pointed satellite of modest sensitivity, and surveys by various groups added

relatively few new Vega-like stars. Decin et al. (2003) give a comprehensive account of these surveys, a major goal of which was characterization of the time dependence of the Vega phenomenon. One limitation of these studies, as noted by Decin et al., is the quite uncertain ages of many of the excess stars. Indeed, we disagree with some of the ages in Table 1 of Decin et al. They describe some limitations to the results presented by Spangler et al. (2001), limitations due, in part, to the poorer than expected sensitivity of ISO.

Most recently, Moor et al. (2006) compiled a list of 60 debris disks with high fractional dust luminosity, $\tau > 10^{-4}$, and within 120 pc of Earth by searching the IRAS and ISO database. 48 objects in Moor et al. are included in our survey while 12 objects are absent. Among those 12 objects missing, four are not Hipparcos stars and 6 of 8 Hipparcos stars did not have a detection at 60 μm with IRAS, therefore, not satisfying our search criteria (§ 3). The remaining two, HD 121812 (HIP 68160) & HD 122106 (HIP 68380), are rejected in this paper due to possible cirrus contamination and the presence of a nearby galaxy, respectively (see Table A4 for the list of rejected sources). We included 5 objects (HIP 13005, HIP 25790, HIP 69682, HIP 77163, & HIP 83480) from the Moor et al. list of rejected suspicious objects; our reasoning is discussed in the notes for these individual objects in Table 2.

Five papers that appeared in 2004 or 2005 report *Spitzer* detections at 70 μm for a total of ~ 20 Vega-like stars that had not previously been detected at 60 μm by IRAS and/or ISO (Meyer et al. 2004; Chen et al. 2005; Beichman et al. 2005; Low et al. 2005; Kim et al. 2005). Although it is not possible to tell exactly how many stars *Spitzer* pointed toward (searched) at 70 μm in these studies, it appears to be of order a few 100. Thus, only about 10% of stars reveal far-IR dust emission at levels between IRAS and *Spitzer* sensitivities.

4. Sample Characteristics

Our IR excess sample consists of 153 Hipparcos dwarfs within 120 pc of Earth. Figure 3 illustrates the distance and $B - V$ distribution of the sample. The relative paucity of debris disks from late-type stars has been previously well established and attributed to the IRAS detection threshold (Song et al. 2002b). However, grain removal by stellar wind drag at M-type stars could also be implicated (Plavchan et al. 2005).

Our stars are listed in Table 2 including 51 out of 58 stars from Paper I. The remaining 7 objects had ISO detections but lacked an IRAS 60 μm detection, an absolute requirement in the present paper. The Hipparcos and the HD numbers are listed in columns (1) and (2). Spectral type, V magnitude and distance from Earth from the Hipparcos main catalog are given in columns (3), (4) and (5). The stellar radius and temperature, R_\star (col. 6) and T_\star (col. 7) are obtained from the SED fit. As described in the previous section, the fitting process was improved from the version used in Paper I and for some objects the best fit R_\star and T_\star deviate slightly from Paper I. For example, HIP 42430 was fit with R_\star of 1.83 R_\odot and T_\star of 5600 K in Paper I, but the improved fit gives R_\star of 1.73 R_\odot and T_\star of 5800 K in Table 2. Our estimations of R_\star are in good agreement with direct measurements such as those with the Very Large Telescope (VLT) interferometer as illustrated in Paper I. The accuracy of our stellar radius measurements is discussed in more detail in a separate paper (Rhee et al. 2006).

A single temperature blackbody fit to the dust component yields T_{dust} (col. 8) for each star, assuming blackbody radiation from dust grains in an optically thin disk. In the case of an IRAS detection at 60 μm , but with only upper limits at 25 μm and 100 μm , we set T_{dust} at 85 K so that the combined flux of the star and dust peaks near 60 μm . This approach leads to a conservative estimate of τ (col. 11), ($= L_{IR}/L_{bol}$). Additional measurements from *Spitzer* and/or ISO were used to better constrain dust temperature for stars in which

such values are available in the literature or from our calculations. (see § 2).

The characteristic orbital semimajor axis of dust particles, R_{dust} , is derived from $R_{dust} = (R_\star/2)(T_\star/T_{dust})^2$ and listed in column (9) in AU. The corresponding angular separation (arcsec) between dust particles and the star is indicated in column (10). The conservative nature of R_{dust} and the angular separation – in the sense that the actual value of R_{dust} at a given star may be substantially larger than the value given in column (9) – is discussed in detail in Paper I. Using a simple model of a thin dust ring (see § 5.1), dust mass (col. 12) was estimated for 61 stars whose dust excess was detected at two or more wavelengths and whose dust radii lie between 9 and 100 AU. Table 2 lists dust mass for a total of 79 stars including 18 stars for which dust mass was directly measured from submillimeter measurements.

Estimation of the age of a star that belongs to a known kinematic stellar group (Zuckerman & Song 2004b) is relatively straightforward. For stars not presently known to be a member of such a group, age estimation is quite difficult and requires cross-checking of several different techniques (Decin et al. 2003; Zuckerman & Song 2004b and references therein). The age estimate and age estimation methods for each star is given in columns (13) and (14). We follow the same lettering convention for each method as indicated in Paper I. A comprehensive review of different techniques of age estimation is found in Zuckerman & Song (2004b).

When available, confirmation of dust excess from MIPS and/or ISO measurements are indicated in column (15) and additional notes for individual objects are marked in column (16). For completeness, we repeat the notes of Table 1 from Paper I in this paper. Finally, a list of rejected sources and the reason for rejection from our survey are presented separately in Table A4.

5. Dust Evolution over Time

Figure 4 illustrates the temporal evolution of τ . The spectral type of each star is represented by the color of each circle, from dark blue for B-type to red for M-type. Circle size reflects the quality of our estimate of age; large, medium and small circles depict good, normal, and low quality age estimates, respectively, as given in column (13) of Table 2. The following list summarizes some characteristics indicated by the distribution of stars in Figure 4.

1. For stars with ages between ~ 10 Myr and 1 Gyr, the maximum τ is a few times 10^{-3} .
2. The percentage of nearby stars with $60 \mu\text{m}$ excess emission detectable by IRAS diminishes with increasing stellar age.
3. The minimum τ is $\sim 10^{-5}$ for early-type (B,A,F) stars and $\sim 10^{-4}$ for later types. This is due to IRAS sensitivity limits and the uncertainty of photospheric flux estimation.
4. At any given age, late-type stars tend to have the largest τ .

As we mentioned in § 3, no pre-2006 analysis of IRAS data is germane to the time evolution of fractional dust excess, τ . By contrast, three teams (Habing et al. 2001; Spangler et al. 2001; Decin et al. 2003) investigated the temporal evolution of the dust using the ISO database. All three studies suffer to some degree from small numbers of detected ISO sources or uncertain/incorrect stellar ages or both. Our IRAS results, Figure 4, are most consistent with the conclusions of Decin et al. (2003) who noticed the regularities listed in items 1-2 above in the ISO data sets they analyzed. In addition, Decin et al. (2003) noticed that there are few young stars with $\tau < 10^{-4}$, which also appears in our Figure 4. This rarity of young low τ stars may be due to the fact that there are not many young early-type stars in solar vicinity (say $\lesssim 50$ pc).

We can roughly quantify item 2 by dividing the IRAS stars into 3 age bins, (A) 10-50 Myr, (B) >50-500 Myr, and (C) >500-5000 Myr. We assume that, in a given volume of space near Earth, stars are uniformly distributed in age for ages up to ~ 1 Gyr. For older stars one first loses all main sequence A-type stars - these evolve off the main sequence in 1 to 2 Gyr - followed by loss of F-type main-sequence stars at ages between ~ 2 to 4 Gyr (Schaller et al. 1992).

Reading from Figure 4, there are 26 stars in bin (A), 78 in bin (B), and 33 in bin (C). By our assumption of equal numbers of stars of any given age in the volume accessible to the sensitivity of IRAS, the age bin (B) contains 10 times more stars in total – with and without a dusty disk – than does bin (A). Since bin (B) in Figure 4 contains about three times the number of Vega-like stars as does bin (A), the probability that a star will be Vega-like is ~ 3 times greater between ages of 10 and 50 Myr than between 50 and 500 Myr.

Similarly, we can estimate the probability that a star in age bin (C) will be Vega-like. We ignore for just a moment the loss of A and F type stars in bin (C) as a result of evolution off the main sequence. In that case, because bin (C) contains 10 times more stars in total – with and without a dusty disk – than does bin (B) but fewer Vega-like stars (33 vs. 78), the probability that a star will be Vega-like in age bin (B) would be ~ 25 times greater than in bin (C). However, because there is a sequential loss of A- and F-type main sequence stars at ages > 1 Gyr, and because these spectral types dominate the IRAS detected $60 \mu\text{m}$ excess stars, we estimate that if a star has an age appropriate for bin (B), then the probability of its being Vega-like is only ~ 8 times (rather than 25 times) greater than the probability of being Vega-like if its age falls in that of bins (C). Then the probability of any given nearby star in age bin (A) being Vega-like is ~ 25 times greater than this probability in bin (C).

The preceding discussion pertains to how the probability of being Vega-like declines with age. We can estimate the absolute value of this probability in two ways. First, two

stars in Table 2 are members of the Hyades (Figure 2: HIP 18975 = VB 160 and HIP 20635 = VB 54). IRAS could have detected excess $60 \mu\text{m}$ emission at Hyades stars with $V \lesssim 6$, which corresponds to a mid-F type star. According to Table 1 in Stern et al. (1995), 40 Hyades members have a V mag brighter than 6. Thus, at an age of 600 Myr, 5% of A-through mid-F type stars in the Hyades are Vega-like above the $60 \mu\text{m}$ flux level accessible to IRAS⁵.

Field A-type stars supply a second sample to estimate the probability that a star will show the Vega-phenomenon. We find, in essential agreement with some previous determinations, that IRAS detected $60 \mu\text{m}$ excess emission at $\sim 20\%$ of A-type stars with $\tau > 10^{-5}$ out to 28 pc (10 of 50 stars) and with $\tau > 4 \times 10^{-5}$ out to 40 pc (22 of 119 stars). The percentage of F-type stars that show the Vega phenomenon at comparable levels of τ appears to be noticeably smaller, but definitive statistics should wait for results from *Spitzer*.

Notwithstanding the much larger probability of a star being Vega-like at young ages, there appears to be very little, if any, distinction with age in peak τ seen in Figure 4 and noted in item 1 above. This suggests that the Vega-phenomenon, at least at the higher levels of τ measured by IRAS, may be mostly the result of occasional large and violent collisional events rather than many small-scale, dust-producing events adding together. For example, there was a very substantial and recent collisional event at the G-type main sequence star BD+20 307, first detected by IRAS at $12 \& 25 \mu\text{m}$ (Song et al. 2005).

Item 4 noted above might be anticipated in a collisional cascade model (cf., Dominik & Decin 2003). In such a model, collisions grind dust particles down to smaller and smaller

⁵Spangler et al. (2001) reported a $60 \mu\text{m}$ ISO detection of Hyades member HIP 20261, but at a flux level, 50 mJy, below the IRAS detection limit.

sizes until sufficiently small particles are blown out of the system by radiation pressure from the star. Lower luminosity, later-type stars will retain more small particles in orbit which in total can possess a large emitting area; thus τ is increased. The larger τ expected for late-type stars in a Dominik & Decin (2003) model is illustrated in their Figure 1f. Earlier, Song (2001) had suggested that late-type stars display larger τ than early-type stars based on the limited data available to him at that time.

5.1. Relationship among τ , Disk Mass, Radius and Stellar Age

Perhaps the quantities of most interest are disk dust mass, disk radial extent, and disk evolution with time. The total mass (M) of dust in a disk may be written:

$$M = \rho N 4\pi a^3 / 3 \quad (7)$$

Where N is the total number of grains in the disk and ρ and a are the density and radius of a typical grain. For an optically thin dusty ring of characteristic radius R ,

$$\tau = N\pi a^2 / 4\pi R^2 \quad (8)$$

Then,

$$\tau/M = 1/\rho a R^2 \quad (9)$$

Thus, if characteristic grain size and density do not vary much among various optically-thin dust disks, then one expects τ/M to vary like the inverse square power of the disk radius, R . Figure 5 shows this to be approximately the case for dust disks with semimajor axes between 10 and 100 AU, where we have taken τ and R from Table 2 and disk mass from the submillimeter literature.

The significance of the filled and open symbols in Figure 5 is as follows. The figure was initially prepared containing only the filled symbols which represent dust mass

determinations based on submillimeter data published prior to 2006. The dashed line was deemed a reasonable “fit” to these solid symbols and we used it to derive disk dust masses for many stars in Table 2 as outlined below. Then, while the present paper was being refereed, a paper presenting submillimeter measured masses for six Table 2 stars appeared (HD 14055, 15115, 21997, 127821, 206893, & 218396; Williams & Andrews 2006). These six stars appear in our Figure 5 as open symbols and, because they line along the dashed line, they clearly indicate the viability of our method.

While recognizing a caveat of statistics of small numbers, the early-type stars preferentially lie above the dashed line and the later type stars below it. This difference could be attributed to smaller grains around the later-type stars (as discussed in § 5). However, this model requires that these grains are sufficiently small that they are unable to radiate like blackbodies at their temperature and thus at a given distance from the star are hotter than blackbody grains would be at that same distance.

Rather few stars appear in Figure 5 as a direct consequence of the limited number of published measurements of submillimeter fluxes for Vega-like stars. In addition, we plot only stars for which far-IR excess emission has been measured in at least two wavelengths; for such stars we can estimate T_{dust} and, thus, R_{dust} .

Because τ is easier to measure (especially with *Spitzer*) than is a submillimeter flux, we use Figure 5 to derive initial estimates of dust masses for many stars listed in column (12) of Table 2. Combining IRAS, ISO and *Spitzer* data, all stars with masses listed in Table 2 and plotted in Figure 6 have measured excess IR emission in at least two wavelengths. As mentioned in § 4 above and emphasized in Paper I, the method used to calculate the values of R_{dust} listed in Table 2 will sometimes substantially underestimate the true R_{dust} . Thus, the Table 2 dust mass estimates should be regarded with some caution.

The solid symbols in Figure 6 indicate a dust mass measurement at submillimeter

wavelengths. We expect that stars plotted with ages $\lesssim 10$ Myr still retain significant amounts of orbiting primordial dust left over from the star formation process. Thus, when considering the evolution of disk masses in dust, these stars should not be compared with the older stars whose dust is of a second generation. Figure 5 in Najita & Williams (2005), based solely on submillimeter data, is suggestive of dust mass decreasing with time. However, when stars with ages $\lesssim 10$ Myr are omitted, the remaining submillimeter data are consistent with constant average dust mass at stars with ages between 30 and 1000 Myr, as suggested by our simple model from Figure 5 and the resulting open points plotted in Figure 6.

Najita & Williams (2005) consider in some detail planet formation models of Kenyon & Bromley (2004a,b). According to the discussion in Najita & Williams, in these models a wave of planet formation in the disk propagates outward generating, as time progresses, dusty debris at successively larger characteristic radii. According to the models, for times perhaps as long as 1 Gyr, the total mass in small grains remains sensibly constant while, in contrast, the reprocessed luminosity (i.e., τ) emitted by the collisional debris begins to decline at a much earlier time ($\lesssim 10$ Myr). This is because, as the wave of planet formation moves outward, grains of a given size subtend increasingly smaller solid angles the further they are located from the star. Comparing our results (Figures 4 & 7) with these models, for ages between 100 and 1000 Myr, little, if any, change is apparent in both τ and the radius R of the debris disk. By contrast, both a decrease in τ and an increase in R appears plausible between 10 and 100 Myr. Should larger samples of debris disks eventually substantiate these results, then the Kenyon & Bromley picture may apply for planet formation times up to, but not much beyond 100 Myr.

Figure 8 is a plot of τ vs. disk radius. The 6 stars with $\tau > 10^{-3}$ all have estimated ages of $\lesssim 20$ Myr. Thus, much of their dust may be a remnant of the star formation process,

rather than second generational. For the other stars, no correlation is apparent between τ and R . Although a grain of a given radius located close to a star will absorb more stellar radiation than one far away, the lifetime of close-in grains might be shorter than for distant grains and these two effects may roughly cancel, on average.

5.2. Algol-type binary stars with far-IR excess emission

An Algol is a binary in which the less massive stellar component fills its Roche lobe and the other, which does not, is not degenerate (Batten 1989). Four stars in Table 2 are eclipsing binaries of the Algol type, including Algol A itself. HIP 76267 was long ago recognized as a $60\text{ }\mu\text{m}$ IRAS excess star (Aumann 1985). The Rieke et al. (2005) *Spitzer* survey at $24\text{ }\mu\text{m}$ included three Algols. For HIP 76267, they report a just-significant, 29%, excess according to their criteria (the *Spitzer* measured flux must be > 1.25 times the expected photosphere to be regarded as significant). Rieke et al. also report a 7% excess at $24\text{ }\mu\text{m}$ for Algol A, although this does not meet their significance threshold of 25%. For HD 40183 their measured $24\text{ }\mu\text{m}$ flux was only 0.88 times the expected photosphere. Although the IRAS FSC reports detection of HD 40183 at 12, 25, and $60\text{ }\mu\text{m}$, we see no evidence of an excess at any wavelength.

The far-IR excess emission at the four Algols might be generated by free-free and bound-free transitions in ionized gas or by cool dust or both. The Algol-type binary stars are susceptible to emission in ionized gas because a small HII region is created around the primary star by material transferred from the secondary star. We first consider far-IR emission in an ionized gas disk orbiting a late B-type primary in Algols listed in Table 3. We assume an electron density $n_e = 10^{10}\text{ cm}^{-3}$ and disk radius $r = 10^{12}\text{ cm}$ (Peters 1989; Guinan 1989). Code et al. (1976) give the flux between 0 and 1100 \AA received at Earth for the B7 star α Leo. This translates to $\sim 2 \times 10^{44}\text{ photons s}^{-1}$ emitted by α Leo and

capable of ionizing hydrogen. The excitation parameter (E), i.e. the number of photons s^{-1} required to maintain an H II region, is

$$E = (4\pi/3)r^3n_e^2\alpha_B \quad (10)$$

(Osterbrock 1974). With $\alpha_B = 2 \times 10^{13} \text{ cm}^3 \text{ s}^{-1}$ at 10,000 K, and $E = 2 \times 10^{44}$ ionizing photons s^{-1} , an H II region with $n_e = 10^{10} \text{ cm}^{-3}$ and radius = 10^{12} cm can be supported.

Considering the four Algols with SEDs displayed in Figure 9, we assume a characteristic distance of 30 pc and a characteristic excess flux at $60 \mu\text{m}$ equal to 0.4 Jy. The orbiting ionized disk described in the preceding paragraph would have a $60 \mu\text{m}$ optical depth ~ 0.2 (Osterbrock 1974) and could account for this excess flux. Thus, it is plausible that ionized gas, rather than dust, could generate the excess far-IR emission in some or even all Algols.

Cool dust might also be present in some of these systems. The fact that Algol itself and HIP 73473 are both triple systems (Worek 2001) may supply a clue as to why cool dust is present at all. In addition to the characteristic mass transfer between primary and secondary, analysis indicates mass is also lost from Algol systems (Batten 1989). If a tertiary component is present, then the system could be analogous in essential respects to binary post-AGB stars, many of which are known to be orbited by a dusty circumbinary disk (e.g., Waters et al. 1991). That is, the central object (a single star in the case of the post-AGB stars and a binary in the case of Algols), ejects mass, some of which is captured into a dusty surrounding disk by the gravity of an orbiting companion.

While such a model might apply to Algol A and to HIP 73473, it need not necessarily apply to other Algols with far-IR excess emission. One obvious test would be a search for evidence of a third star in the HIP 21604 and HIP 76267 systems.

6. Summary and Conclusions

The 1983 all-sky IRAS far-infrared survey yielded a wealth of information about the properties of cool dust in orbit around main sequence stars. However, notwithstanding decades of ground- and space-based follow-up projects including ISO, as of 2004 when we began the research reported here, in our opinion, a consistent, convincing evolutionary picture of these dusty stars had not been published. In particular, while various researchers had cross-correlated various stellar catalogs against the IRAS catalog, none had utilized the Hipparcos catalog. Stellar distances and proper motions provided by the Hipparcos and Tycho catalogs yield information useful for establishing ages of dusty stars; reliable ages are essential if correct evolutionary sequences are to be deduced. Also, as a consequence of the rather large IRAS beam-size and inadequate attention to elimination of background confusion, some previous stellar studies with IRAS have suffered from the inclusion of false positive far-IR excess stars.

In the research reported here we have taken special pains to deduce stellar ages and to eliminate false positives. Just as it is possible to deduce many properties of stellar clusters and associations even though some stars are mistakenly included as members, we trust that our Table 2 IRAS sample is clean enough that our conclusions will stand the test of time. Nonetheless, because ages of nearby field stars are notoriously difficult to estimate accurately and because of limitations with the IRAS database, we recognize that some entries in the tables and figures presented in this paper will be in error.

IRAS was most effective for the study of luminous B- and A-type main sequence stars. In agreement with some earlier studies, we find that IRAS detected excess emission at $60\text{ }\mu\text{m}$ from about 20% of nearby A-type stars. This percentage will certainly rise as the A-stars are examined with far-IR photometers more sensitive than those aboard IRAS. In particular, we find that about 10% of stars of various spectral classes are revealed to

display far-IR dust emission at brightness levels between IRAS and *Spitzer* sensitivities. Although this 10% subsumes stellar age, spectral types and distance from Earth and thus is potentially subject to selection effects, it is consistent with the well-defined TW Hydra Association sample of Low et al. (2005). Using heterogeneous samples, Smith et al. (2006) and Bryden et al. (2006) also reported about 10% of stars show dust excess in the MIPS 70 μm band, but below IRAS sensitivity.

From their analysis of ISO data sets, especially the volume-limited sample of Habing et al. (2001), Decin et al. (2003) deduced that the percentage of stars with detectable 60 μm emission diminishes with age. However, the small data set of Habing et al. (2001) and difficulties with estimating stellar age, precluded a meaningful quantitative result in our opinion. With our larger and more robust database we can derive that the probability of 60 μm excess emission detectable with the sensitivity of IRAS is about 25 times larger for A- and F-type stars with ages in the range 10-50 Myr compared to such stars with ages > 500 Myr within the volume within 120 pc of Earth.

While it is generally agreed that measurements at submillimeter wavelengths are best for the derivation of dust masses, by means of a simple model that relates submillimeter and far-IR fluxes, we are able to derive dust masses for numerous stars that lack submillimeter data. These masses lie in the range between 0.0005 and 0.5 M_{\oplus} . For stars with ages between 30 and 1000 Myr, these dust masses appear to depend little, if at all, on age. Based on Figure 5, and as described in § 5.1, our model indicates that far-IR data can be used, quite reliably, to predict a submillimeter flux and, thus, a disk dust mass. As a consequence, disk dust masses can generally be derived based solely on *Spitzer* data provided that excess flux is measured at two or more well separated wavelengths with MIPS and/or IRS.

Four Algol binary stars appear to display excess emission at 60 μm wavelength, although the existence of the excess is perhaps not compelling in all cases. We considered

models where the emission is generated by free-free and bound-free emission in orbiting ionized gas or by orbiting dust particles, dust perhaps associated with a tertiary (third) stellar component. Future studies will be required to clarify the dominant physical mechanism(s) involved.

We thank the referee for his/her constructive comments that helped to improve this paper. We also thank Travis Barman for providing a customized set of Next Gen. Phoenix models of stellar atmospheres, and M. Jura for helpful comments. This research has made use of the VizieR catalogue access tool, CDS, Strasbourg, France and of data products from the Two Micron All Sky Survey (The latter is a joint project of the University of Massachusetts and the Infrared Processing and Analysis Center/California Institute of Technology, funded by the National Aeronautics and Space Administration and the National Science Foundation). JR acknowledges a NASA grant NAG-13067 for financial support.

A. Appendix material

Table A4. List of Rejected Sources

HIP	HD	IRAS Source	Contamination Source	Additional Data Source	Reason of Rejection [†]
1468	1407	F00157+1907	UGC 00169	NED	1
2021	2151	F00235-7731			2
8796	11443	F01502+2919			2
8817	...	F01506+2312	2MASX J01532347+2327067	NED	1
9236	12311	F01572-6148			2
12361	16743	F02374-5308			3
12843	17206	F02427-1846		MIPS	4
13847	18622	F02563-4030			2
14897	20010	F03095+1351			2
15197	20320	F03134-0900			2
16276	20110	F03190+8352	HIP 16267		5
17378	23249	F03408-0955			2
17439	23484	F03423-3826		ISO	6
17531	23338	03421+2418			6,7
17573	23408	F03428+2412	NGC 1432	NED	1
17579	23432	03429+2423			6,7
17608	23480	F03433+2347			6,7
17921	23950	F03469+2205			6,7
22449	30652	F04471+0652			2
23818	33095	F05049-1927			1
25110	33564	F05142+7911	IRAS F05142+7911	MIPS	1
25732	36150	05271-0050			6
27100	39014	F05446-6545			6
28103	40136	F05541-1410		MIPS	2
28360	40183	F05558+4456			2
30252	44958	F06207-5112			8
32277	...	F06407+4040	HIP 32275		5
32349	48915	06429-1639			2
32435	53842	F06539-8355		MIPS	9
34473	55864	F07091-7024			2

Table A4—Continued

HIP	HD	IRAS Source	Contamination Source	Additional Data Source	Reason of Rejection [†]
35457	56099	F07149+5913		MIPS	9
35789	58853	F07225-6432		IRAS F07225-6432	1
37279	61421	F07366+0520		MIPS	2
40167	68255	F08093+1747			10
43100	74738	F08436+2856	HIP 43103		5
44923	78702	F09067-1807		MIPS	6
44915	78752	F09068-2844			6
45238	80007	F09126-6930			2
46853	82328	F09294+5154			2
46984	82821	F09319+0346	2MASX J09343627+0332421	NED	1
49669	87901	F10057+1212			2
54835	97455	F11107+5541	SBS 1110+556	NED	1
57583	...	F11457-2150			3
57757	102870	F11481+0202			2
58001	103287	F15512+5358			2
58364	103913	11554+2524		NED	1
59307	105686	F12074-3425	GdF J1209598-344142	NED	1
60112	107228	F12171+0549	NGC 4266	NED	1
60902	108653	F12263+0126	SDSS J122856.95+010907.4	NED	1
61932	110304	F12387-4841			2
61941	110379	F12390-0110			2
61947	...	F12394+4319	2MASX J12414864+4302494	NED	1
62956	112185	F12518+5613			2
63973	113767	13036-4924	NGC 4945A	NED	1
65109	115892	F13177-3627		MIPS	2
65378	116656	F13219+5511			2
66249	118098	F13321-0020		ISO	2
67927	121370	F13522+1838			2
68160	121812	F13549+2336			6
68380	122106	F13571-0318	APMUKS(BJ) B135713.55-031828.8	NED	1

Table A4—Continued

HIP	HD	IRAS Source	Contamination Source	Additional Data Source	Reason of Rejection [†]
70497	126660	F14235+5204			2
72339	130322	F14449-0004	APMUKS(BJ) B144458.55-000415.4	NED	1
72659	131156	F14491+1918			2
75039	136580	F15182+4109	2MASX J15200834+4059114	NED	1
76641	139907	F15374+4401	UGC 09959	NED	1
77634	141556	15477-3328			6
78072	142860	F15541+1548		MIPS	2
78527	144284	F16009+5841			2
78594	143840	F16001-0440		MIPS	9
79807	147094	F16159+5229	2MASX J16171300+5222153	NED	1
81693	150680	F16393+3141			2
83343	...	F16599+2300			11
84696	156635	F17162-0245			1
85104	...	F17223+4811			8
85576	158373	F17265-0957		ISO	6
85790	159139	17299+2826	CGCG 170-036	NED	1
86032	159561	F17326+1235			2
86974	161797	F17444+2744			2
87815	164330	F17559+6236		ISO	6
89937	170153	F18220+7242			2
92683	174966	18505+0141			12
93371	176270	F18576-3708	IC 4812	NED	1
93449	...	F18585-3701	NGC 6729	NED	1
98433	189478	19575+0647			6
99240	190248	F20039-6619			2
105090	202560	F21141-3904		MIPS	2
105858	203608	F21223-6535		MIPS	2
106368	204942	F21297-2422	APMUKS(BJ) B212943.47-242303.3	NED	1
107556	207098	F21442-1621			2
108594	...	F21563-6220	APMUKS(BJ) B215622.59-622020.9	NED	1

Table A4—Continued

HIP	HD	IRAS Source	Contamination Source	Additional Data Source	Reason of Rejection [†]
108870	209100	F21598-5700		MIPS	2
111278	213617	F22301+1958		ISO/MIPS	6
111544	214168	F22335+3921	HIP 111546		5
111558	...	F22330-5154	ESO 238-IG 019	NED	1
114996	219571	F23145-5830		ISO	2
118182	...	F23558+5106	HIP 118188		5
118268	224617	F23567+0634			6

Note. — Unless already confirmed by additional instruments, those objects rejected because of possible cirrus contamination need confirmation from *Spitzer* MIPS 70 μ m measurement.

[†] 1. There exists a nearby extended source within 3σ IRAS positional error ellipse.
 2. SED shows that IRAS 60 μ m or MIPS 70 μ m detection falls on the stellar photosphere.
 3. IRAS FSC long format indicates a large offset between 60 μ m and 12 μ m positions.
 4. No source was detected at the expected stellar position in MIPS 70 μ m image.
 5. There exists a bright star within 3σ IRAS positional error ellipse.
 6. IRAS 60 μ m excess is likely caused by cirrus contamination.
 7. This star is a member of the Pleiades cluster.
 8. 3σ IRAS positional error ellipse does not include the target star.
 9. Moor et al. (2006) rejected this star based on their *Spitzer* MIPS observation.
 10. Infrared excess had $< 2.5\sigma$ detection at IRAS 60 μ m band (see § 3 for the definition of σ).
 11. *Spitzer* MIPS 70 μ m image shows extended emission.
 12. There exists a huge background galaxy behind this star.

REFERENCES

Aumann, H. H. 1985, PASP, 97, 885

Aumann, H. H., Gillett, F. C., Beichman, C. A., de Jong, T., Houck, J. R., Low, F. J., Neugebauer, G., Walker, R. G., & Wesselius, P. R. 1984, ApJ, 278, L23

Backman, D. E., & Paresce, F. 1993, in Protostars and Planets III, ed. V. Mannings, A.P. Boss, & S. S. Russell (Tucson: Univ. Arizona Press), 1253

Batten, A. H. 1989, in “Algols”, ed A.H. Batten, Kluwer Academic Publishers, Dordrecht, p. 1

Beckwith, S. V. W., Henning, T., & Nakagawa, Y. 2000, in Protostars and Planets IV, ed. V. Mannings, A. P. Boss, & S. S. Russell (Tucson: Univ. Arizona Press), 533

Beichman, C. A., Bryden, G., Rieke, G. H., Stansberry, J. A., Trilling, D. E., Stapelfeldt, K. R., Werner, M. W., Engelbracht, C. W., Blaylock, M., Gordon, K. D., Chen, C. H., Su, K. Y. L., & Hines, D. C. 2005, ApJ, 622, 1160

Bessell, M. 2000, PASP, 112, 961

Bryden, G. et al. 2006, ApJ, 1098, 1113

Chen, C. H., Patten, B. M., Werner, M. W., Dowell, C. D., Stapelfeldt, K. R., Song, I., Stauffer, J. R., Blaylock, M., Gordon, K. D., & Krause, V. 2005, ApJ, 634, 1372

Code, A.D., Bless, R.C., Davis, J. & Brown, R.H. 1976, ApJ, 203, 417

Cox, A. N., ed., 2000 Allen’s Astrophysical Quantities. AIP Press and Springer, New York

Decin, G., Dominik, C., Waters, L. B. F. M., & Waelkens, C. 2003, ApJ, 598, 636

Dominik, C. & Decin, G. 2003, ApJ, 598, 626

Guinan, E.F. 1989, in “Algols”, editor A.H. Batten, Kluewer Academic (Dordrecht), 35

Habing, H. J., Dominik, C., Jourdain de Muizon, M., Laureijs, R. J., Kessler, M. F., Leech, K., Metcalfe, L., Salama, A., Siebenmorgen, R., Trams, N., & Bouchet, P. 2001, *A&A*, 365, 545

Hauschildt, P. H., Allard, F., & Baron, E. 1999, *ApJ*, 512, 377

Jura, M., et al. 2004, *ApJS*, 154, 453

Kalas, P., Graham, J. R., Beckwith, S. V. W., Jewitt, D. C., & Lloyd, J. P. 2002, *ApJ*, 567, 999

Kenyon, S. J. & Bromley, B. C. 2004a, *AJ*, 127, 513

Kenyon, S. J. & Bromley, B. C. 2004b, *ApJ*, 6081602, L133

Kim J. et al. 2005, *ApJ*, 632, 659

Kouwenhoven, M. B. N., Brown, A. G. A., Zinnecker, H., Kaper, L., & Portegies Zwart, S. F. 2005, *A&A*, 430, 137

Lagrange, A. M., Backman, D. E., & Artymowicz, P. 2000 in *Protostars and Planets IV*, eds. Mannings, V., Boss, A. P., Russell, S. S. (Tucson: University of Arizona Press), 639

Low, F. J., Smith, P. S., Werner, M., Chen, C., Krause, V., Jura, M., & Hines, D. C. 2005, *ApJ*, 631, 1170

Lowrance, P. J., et al. 2000, *ApJ*, 541, 390

Meyer, M. R. et al. 2004, *ApJS*, 154, 422

Moor, A., Abraham, P., Derekas, A., Kiss, Cs., Kiss, L. L., Apai, D., Grady, C., Henning, Th. 2006, astro-ph/0603729

Najita, J. & Williams, J. P. 2005, ApJ, 635, 625

Odenwald, S. F. 1986, ApJ, 307, 711

Osterbrock, D.E. 1974, "Astrophysics of Gaseous Nebulae", W.H. Freeman & Company, San Francisco, 21 & 79

Peters, G.J. 1989, in "Algols", editor A.H. Batten, Kluewer Academic (Dordrecht), 9

Plavchan, P., Jura, M., Lipsky, S. J. 2005, ApJ, 631, 1161

Pollack, J. B., Hollenbach, D., Beckwith, S., Simonelli, D. P., Roush, T., & Fong, W. 1994, ApJ, 421, 615

Rhee, J. H., Kim, S., & Song, I. 2006, ApJ, in preparation

Rieke G.H. et al. 2005, ApJ, 620, 1010

Schaller, G., Schaerer, D., Meynet, G., & Maeder, A. 1992, A&AS, 96, 269

Silverstone M. 2000, *The Vega phenomenon: evolution and multiplicity*. PhD thesis. Univ. Calif., Los Angeles. 194 pp.

Smith, P. S., Hines, D. C., Low, F. J., Gehrz, R. D., Polomski, E. F., Woodward, C. E. 2006, ApJ, 644, L125

Song, I. 2001, in ASP Conf. Ser. 244, Young Stars Near Earth: Progress and Prospects, ed. R. Jayawardhana & T. Greene (San Francisco: ASP), 221

Song, I., Bessell, M. S., & Zuckerman, B. 2002a, A&A, 385, 862

Song, I., Caillault, J. -P., Barrado y Navascues, D., & Stauffer, J. R. 2000, ApJ, 533, L41

Song, I., Weinberger, A., J., Becklin, E. E., Zuckerman, B., & Chen, C. 2002b, *ApJ*, 124, 514

Song, I., Zuckerman, B., & Bessell, M. S. 2003, *ApJ*, 599, 342

Song, I., Zuckerman, B., Weinberger, A. J., Becklin, E. E. 2005, *Nature*, 436, 363

Spangler, C., Sargent, A. I., Silverstone, M. D., Becklin, E. E., & Zuckerman, B. 2001, *ApJ*, 555, 932

Stauffer, J. R. et al. 2005, *AJ*, 130, 1834

Stern, R. A., Schmitt, J. H. M. M., Kahabka, P. T. 1995, *ApJ*, 448, 683

Waters, L.B.F.M., Trams, N. R., Waelkens 1991, in "The Infrared Spectral Region of Stars", eds C. Jaschek & Y. Andrillat, Cambridge University Press, p. 40

Williams, J. P. & Andrews, S. M. 2006, *astro-ph/0609122*

Worek, T. F. 2001, *PASP*, 113, 964

Zuckerman, B. 2001, *ARA&A*, 39, 549

Zuckerman, B., Forveille, T., & Kastner, J. H. 1995b, *Nature*, 373, 494

Zuckerman, B., Kim, Sungsoo S., Liu, T. 1995a, *ApJ*, 446, L79

Zuckerman, B., & Song, I. 2004a, *ApJ*, 603, 738 (Paper I)

Zuckerman, B., & Song, I. 2004b, *ARA&A*, 42, 685

Zuckerman, B., Song, I., Bessell, M. S., & Webb, R. A. 2001a, *ApJ*, 562, L87

Zuckerman, B., Song, I., & Webb, R. A. 2001b, *ApJ*, 559, 388

Zuckerman, B., & Webb, R. A. 2000, *ApJ*, 535, 959

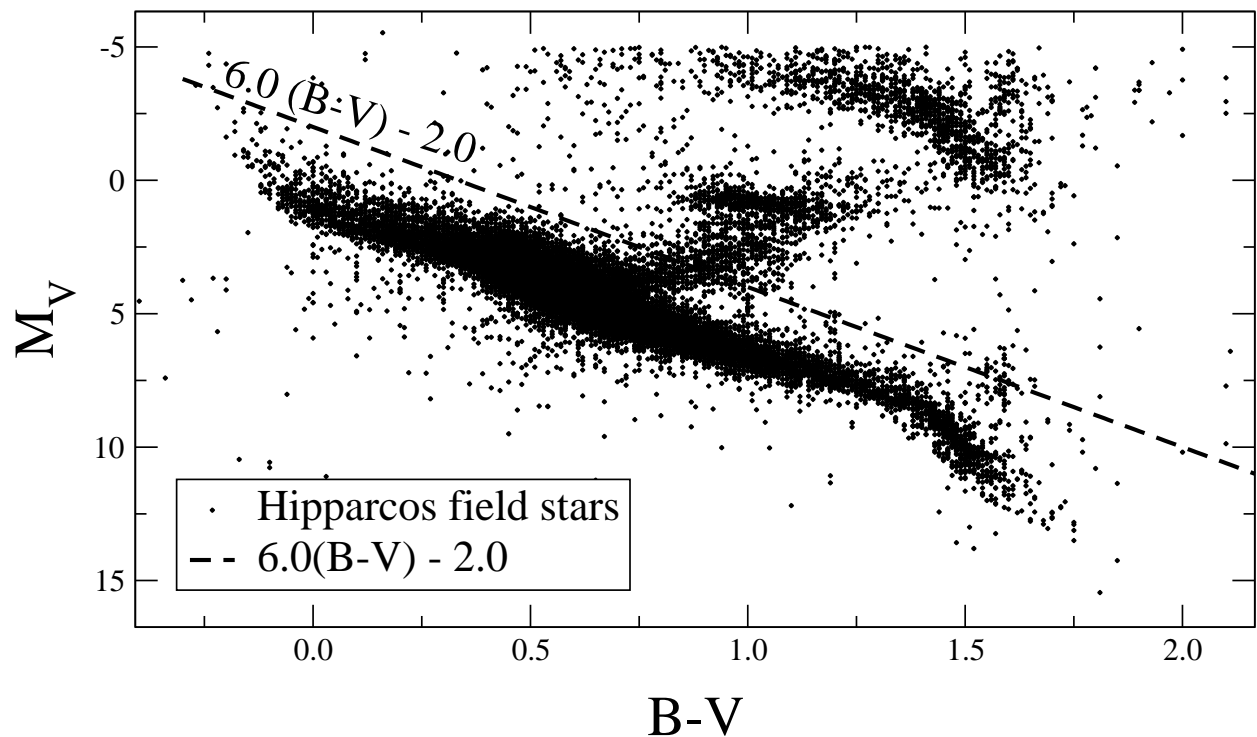


Fig. 1.— HR diagram of Hipparcos field stars. Stars below the dashed line have been searched for IRAS 60 μ m excess emission.

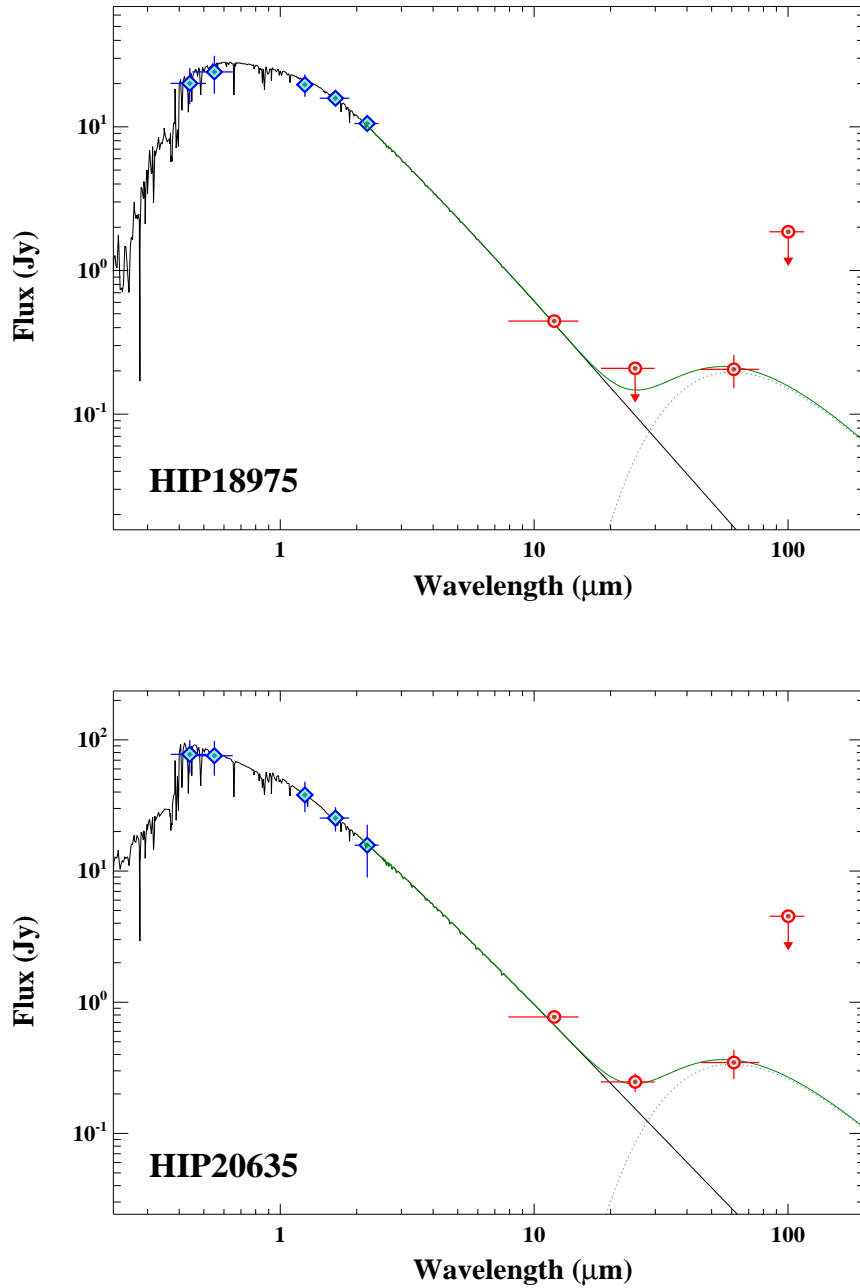


Fig. 2.— Spectral Energy Distribution (SED) of Hyades stars. Fitting parameters (e.g., R_* , T_* , R_{dust} , T_{dust}) of each star are given in Table 2. SEDs of the remaining IR excess stars are available in the electronic edition.

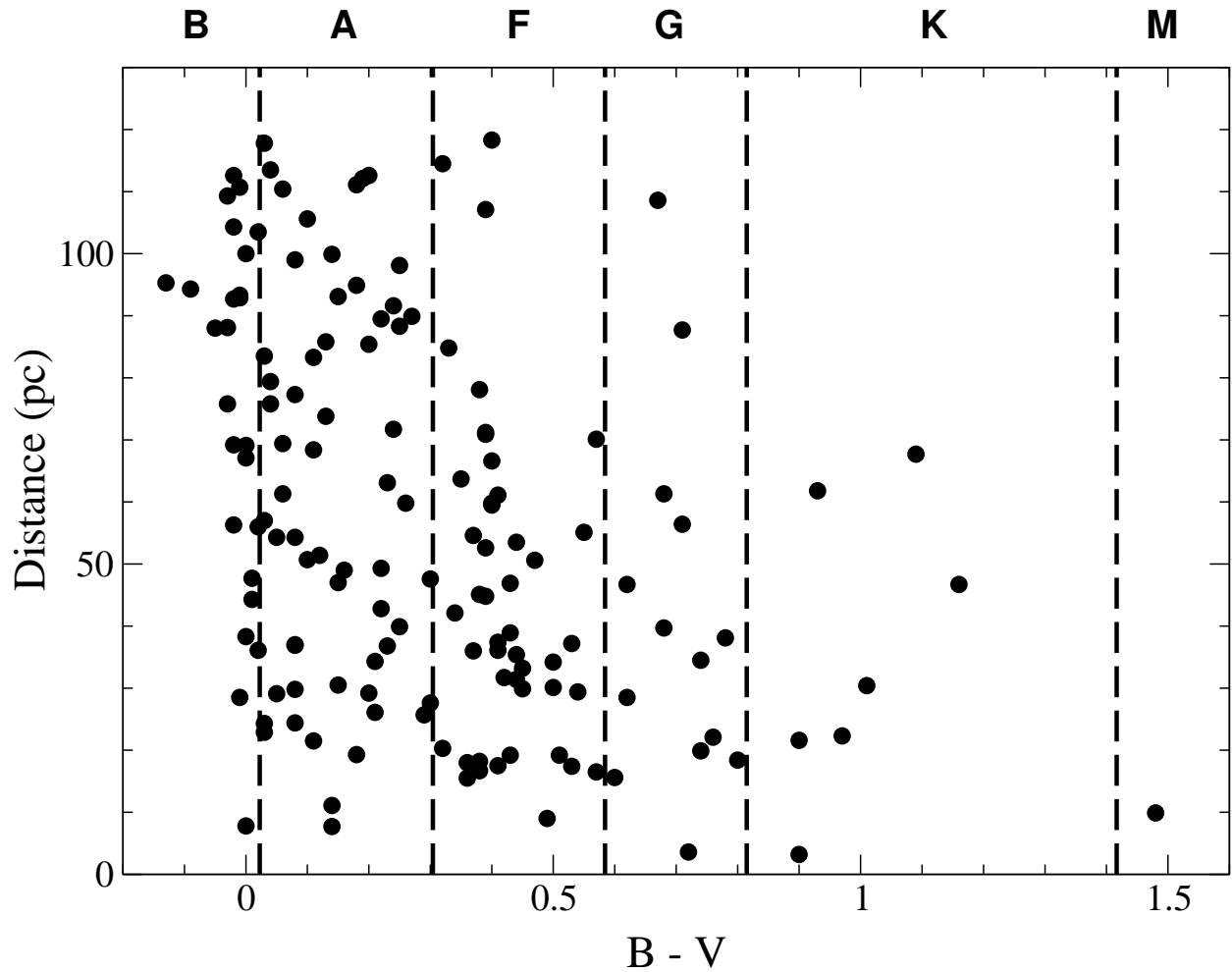


Fig. 3.— Distribution of our candidate excess stars in distance from Earth as a function of $B-V$. As reported before, early type stars dominate the IRAS debris disk systems.

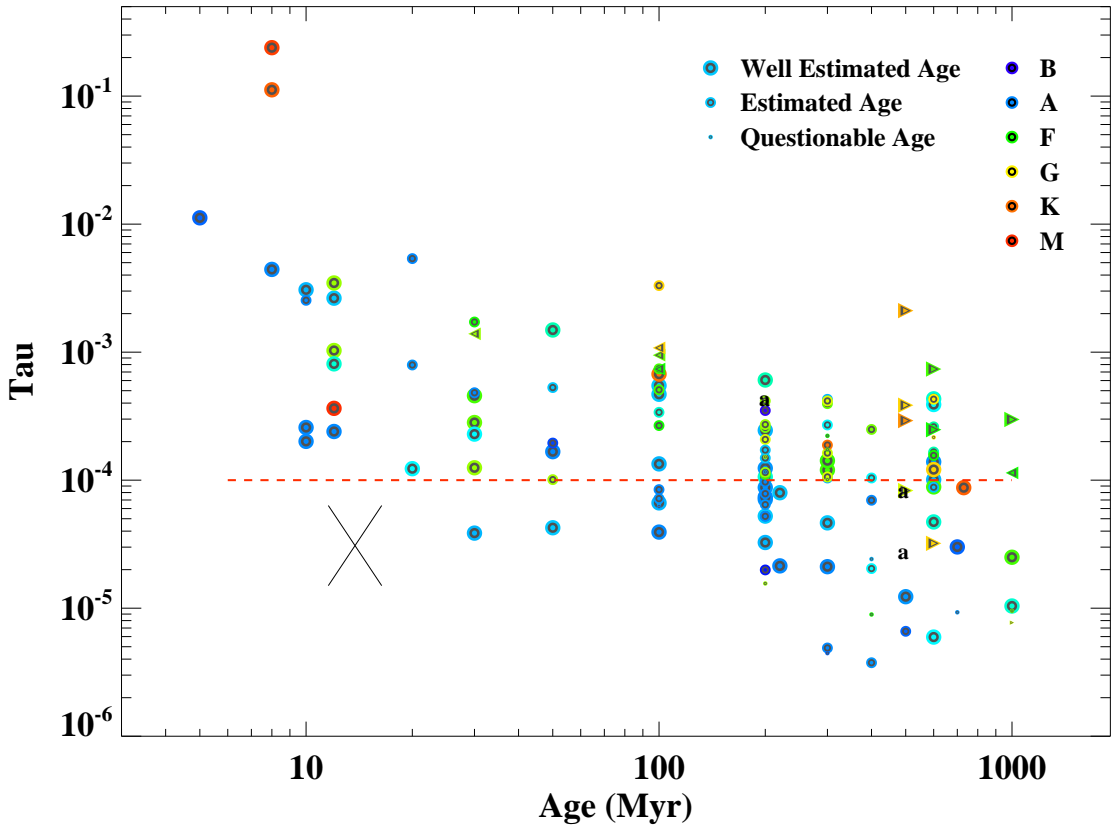


Fig. 4.— τ as a function of stellar age. Plotted lower case “a” are Algol-type stars. Well estimated age, estimated age, and questionable age correspond respectively to zero, one, and two question marks in column (13) of Table 2. Stars with cautions noted in Table 2 for possible contamination are not plotted in the figure.

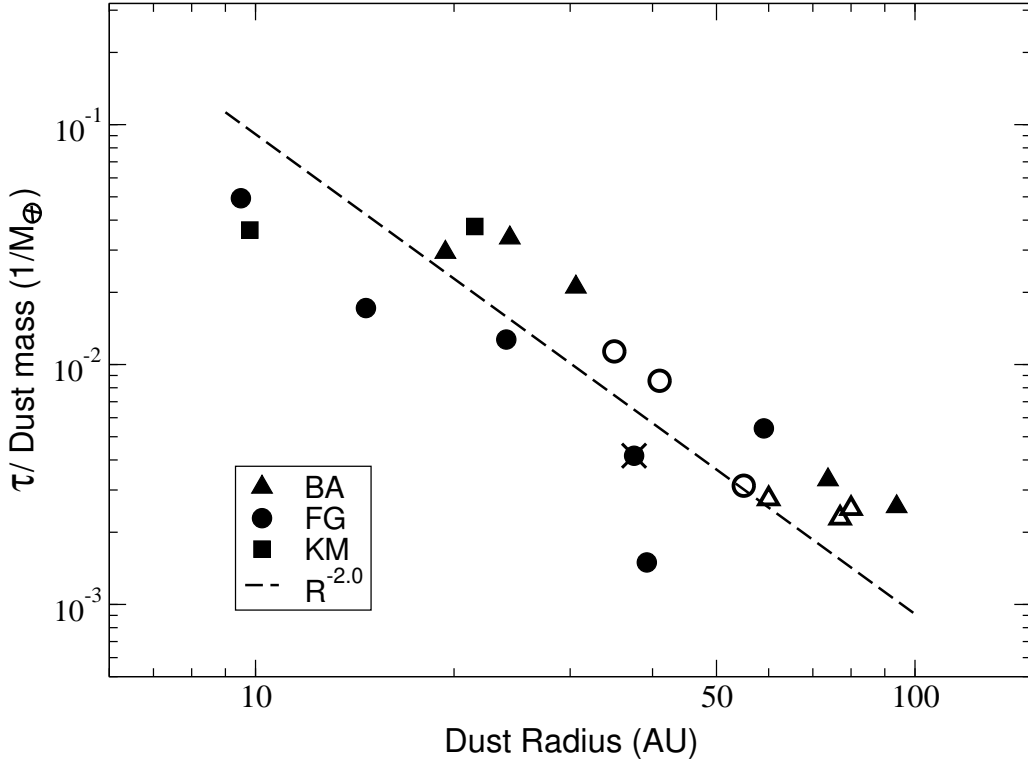


Fig. 5.— τ/M_{dust} as a function of dust radius (AU). M_{dust} , given in Earth masses (M_{\oplus}), is derived from submillimeter measurements reported in the published literature. The filled and open symbols represent dust mass determinations based on submillimeter data published prior to 2006 and during 2006, respectively. See § 5.1 for further discussion of these data. To achieve consistency among data reported in various published papers, all masses given in the plot have been normalized (by us) to have a dust opacity of $1.7 \text{ cm}^2 \text{ g}^{-1}$ at $850 \mu\text{m}$ and dust temperature as given in our Table 2. However, uncertainties in the $850 \mu\text{m}$ dust opacity caused by different grain sizes and compositions can result in the over- or underestimate of dust mass by a factor of three or so (e.g., Pollack et al. 1994; Beckwith et al. 2000). Meanwhile, the relative masses of the various submillimeter determinations might be better constrained than their absolute values if each star has reasonably similar dust. In our plot, the relative masses are probably trustworthy to about a factor of two. All stars plotted have measured far-IR excess emission in at least two wavelengths. τ for one star (HD 104860) is from ISO, not IRAS, and is marked “ \times ”.

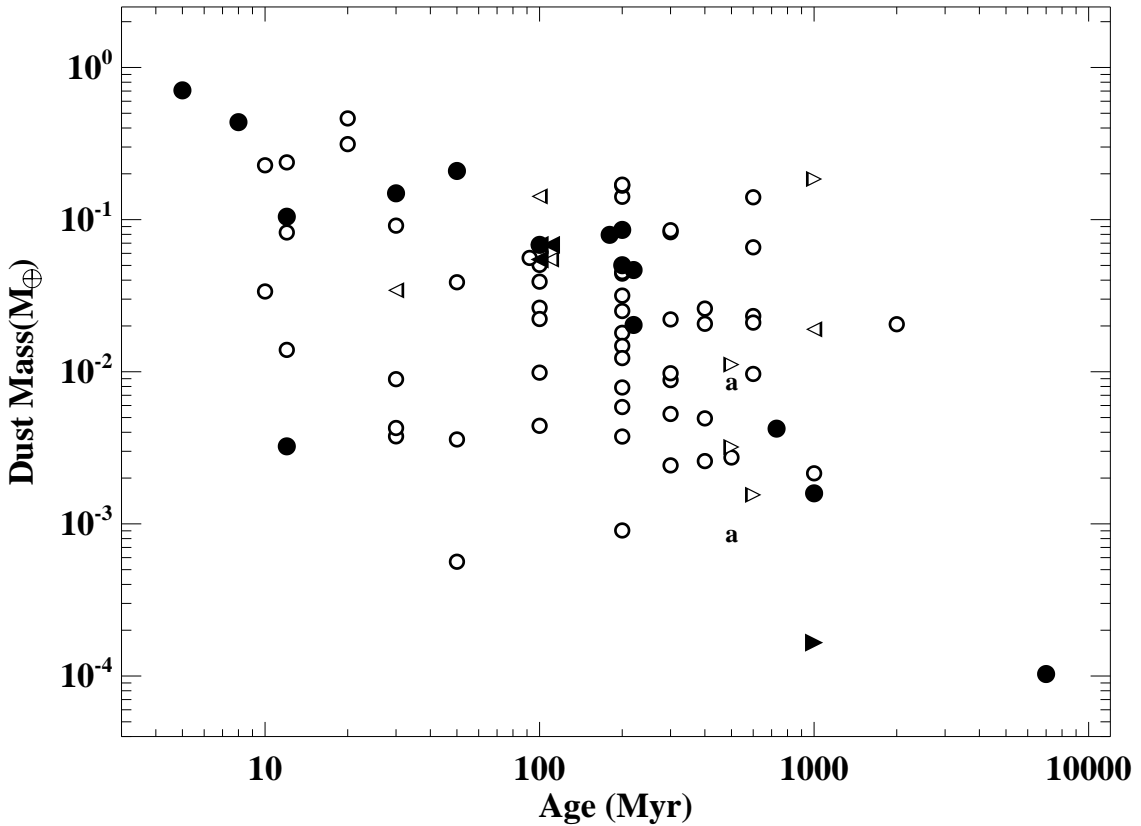


Fig. 6.— M_{dust} as a function of stellar age. Solid symbol depicts M_{dust} obtained from submillimeter measurements while open symbol represents M_{dust} derived from Figure 5 (see § 5.1). All stars plotted have measured far-IR excess emission in at least two wavelengths and R_{dust} between 9 and 100 AU. Two Algol-type stars are plotted with lower case “a” (although their IR excess may not be due to dust particles, see § 5.2).

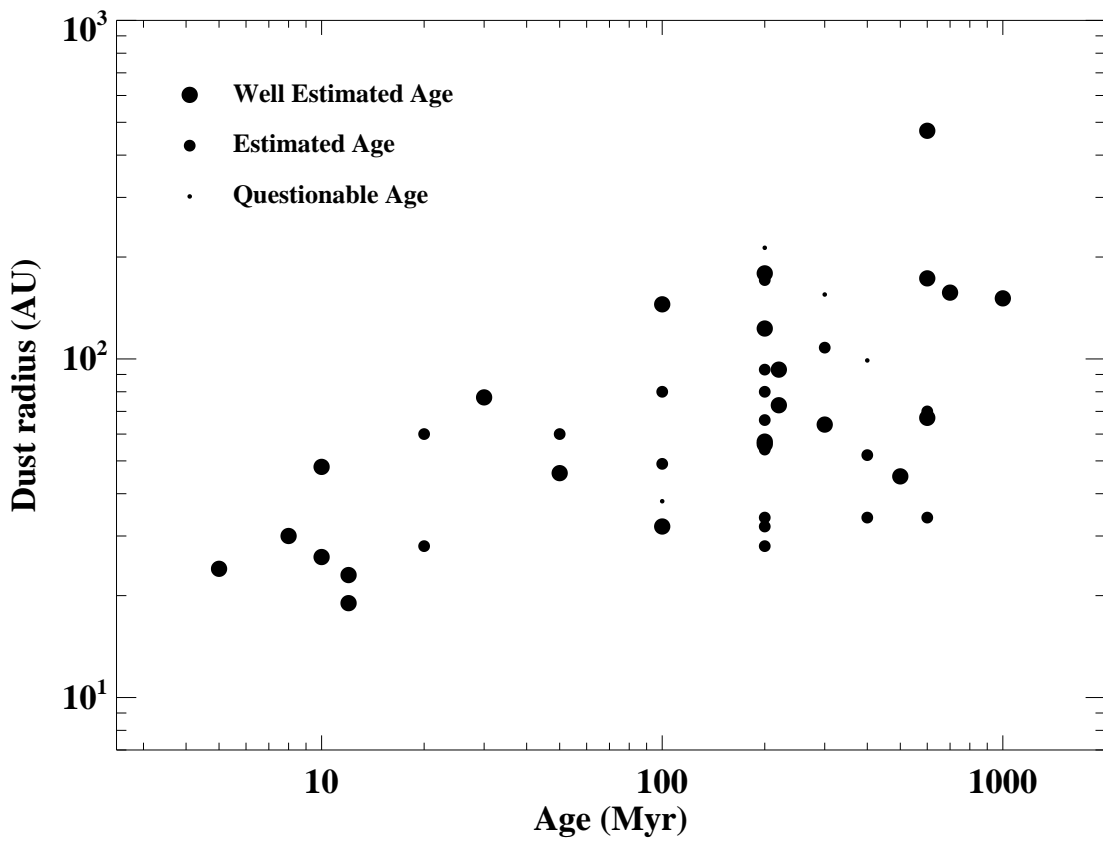


Fig. 7.— Dust radii of early type IR excess stars (B & A) as a function of stellar age. All stars plotted have measured far-IR excess emission in at least two wavelengths.

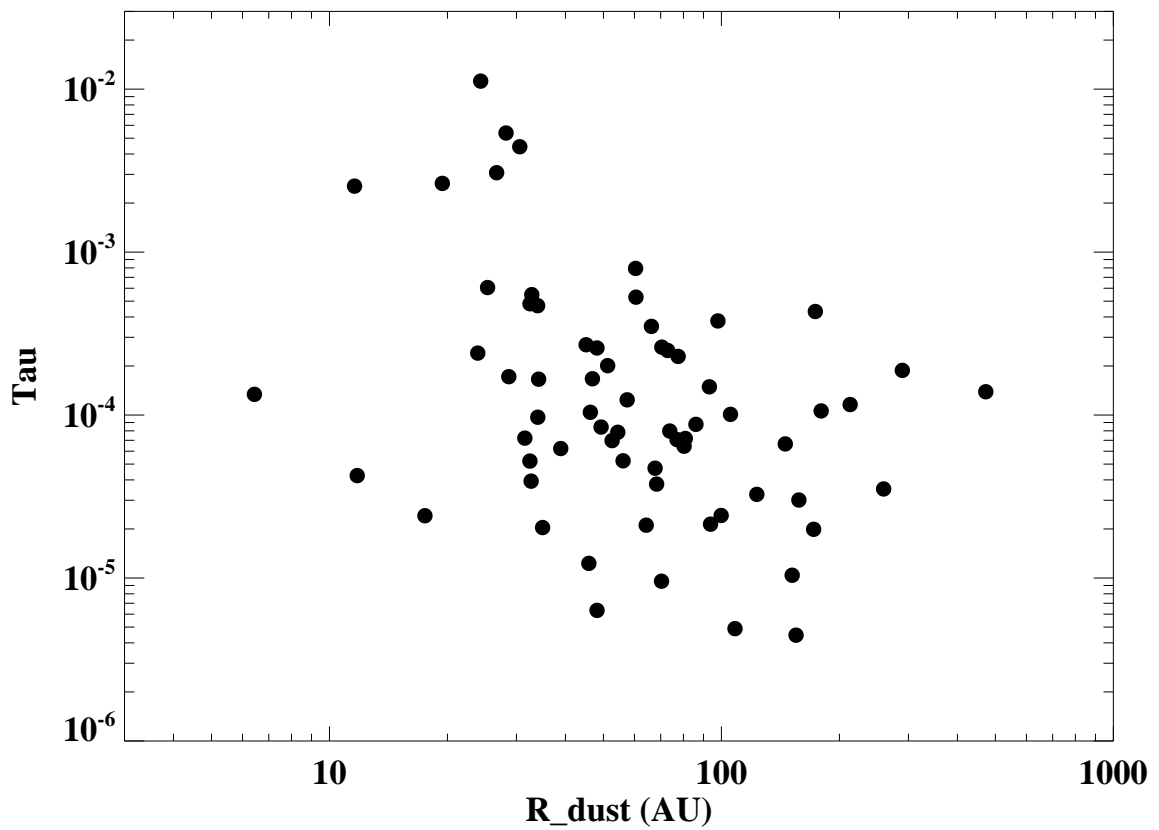


Fig. 8.— τ of early type IR excess stars (B & A) as a function of dust radii. All stars plotted have measured far-IR excess emission in at least two wavelengths.

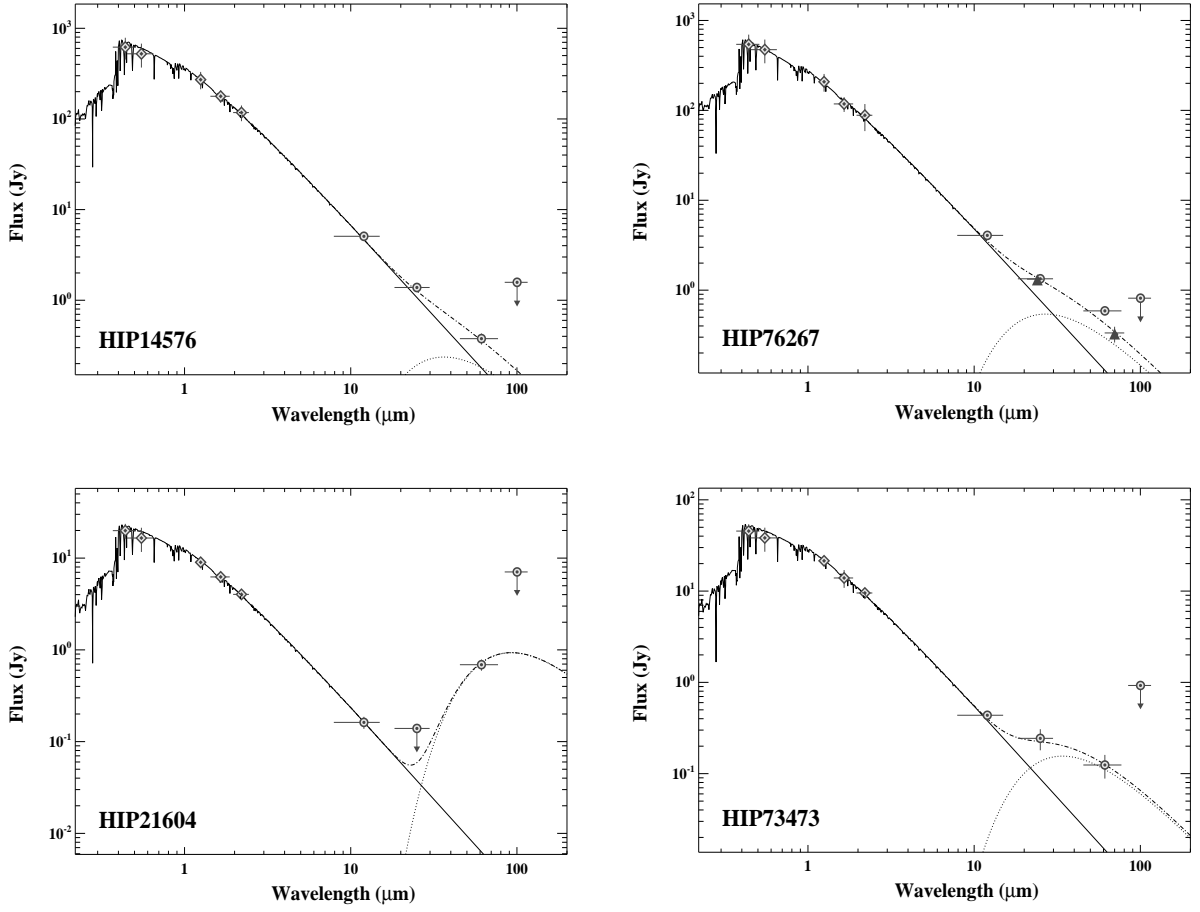


Fig. 9.— Spectral Energy Distribution (SED) of Algol-type stars. For HIP 76267 the filled triangle data points at 24 and 70 μm are from Rieke et al. (2005). Fitting parameters (e.g., R_\star , T_\star , R_{dust} , T_{dust}) of each star are given in Table 2. However, the far-IR emission might be generated by ionized gas (see § 5.2).

Table 1. Hipparcos Class I & II Pre-main Sequence Stars within 120 pc

HIP	HD	Other	Sp. Type	V	Distance
				(mag)	(pc)
17890	275877	XY Per	A2IIev	9.44	120.0
23873	240764	RW Aur A	G5V:e...	10.3	70.5
26295	36910	CQ Tau	F2IVe	10.7	99.5
56354	100453	...	A9Ve	7.79	111.5
56379	100546	KR Mus	B9Vne	6.70	103.4
58520	104237	DX Cha	A:pe	6.60	116.1
82323	...	V1121 Oph	K5	11.25	95.1

Table 2. Stars with Dusty Debris Disks

				V	D	R_\star	T_\star	T_{dust}	R_{dust}	angle	Dust mass	age	Age	Dust Excess	
HIP	HD	Sp. Type	(mag)	(pc)	(R_\odot)	(K)	(K)	(AU)	(arcsec)	τ	M_\oplus	(Myr)	Method [†]	Confirmation	Notes ^α
(1)	(2)	(3)	(4)	(5)	(6)	(7)	(8)	(9)	(10)	(11)	(12)	(13)	(14)	(15)	(16)
746	432	F2III-IV	2.3	16.7	3.36	7200	120	28	1.68	2.50E-05	2.15E-03	1000	a,b,c	...	
1185	1051	A7III	6.8	88.3	1.87	8000	40	173	1.97	4.32E-04		600	a,d	...	
4267	5267	A1Vn	5.8	112.6	2.67	10000	85	86	0.76	8.77E-05		200	a,d	...	1,2
5626	6798	A3V	5.6	83.5	2.25	10000	75	93	1.12	1.49E-04	1.41E-01	200?	a,d	...	
6686	8538	A5Vv	2.7	30.5	3.90	8400	85	88	2.90	5.95E-06		600	a,d	...	
6878	8907	F8	6.7	34.2	1.19	6600	45	59	1.74	2.08E-04	3.84E-02 [‡]	200?	a,b,c	MIPS/ISO	
7345	9672	A1V	5.6	61.3	1.66	10000	80	60	0.99	7.94E-04	3.13E-01	20?	ZFK	...	3
7805	10472	F2IV/V	7.6	66.6	1.28	7000	85	20	0.30	4.57E-04		30	ZSW	...	
7978	10647	F8V	5.5	17.4	0.99	6400	65	22	1.28	4.16E-04	2.21E-02	300?	a,b,c	...	
8102	10700	G8V	3.5	3.6	0.79	5400	75	9	2.60	1.16E-05	2.35E-04 [‡]	7000?	a,b	ISO	
8122	10638	A3	6.7	71.7	1.57	8200	85	33	0.47	4.69E-04		100	a,d	...	
8241	10939	A1V	5.0	57.0	1.94	10000	75	80	1.41	6.44E-05	4.52E-02	200?	a,d	MIPS	2,4
9570	12471	A2V	5.5	113.5	3.28	10000	85	105	0.93	1.01E-04		600	a,d	...	
10054	12467	A1V	6.0	68.4	1.73	9200	40	213	3.11	1.16E-04		200??	a,d	...	2
10670	14055	A1Vnn	4.0	36.1	1.96	10000	75	80	2.24	7.18E-05	2.86E-02 [‡]	100?	a,d	...	
11360	15115	F2	6.8	44.8	1.23	7200	65	35	0.78	5.08E-04	4.48E-02 [‡]	100?	a,b,c	MIPS/ISO	
11486	15257	F0III	5.3	47.6	2.26	7400	85	39	0.84	1.14E-04	1.90E-02	\lesssim 1000	a,d	...	2
11847	15745	F0	7.5	63.7	1.21	7600	85	22	0.35	1.72E-03	9.13E-02	30?	d	MIPS/ISO	
12964	17390	F3IV/V	6.5	45.1	1.39	7200	50	67	1.49	1.73E-04	8.52E-02	300??	a	...	
13005	...	K0	8.1	67.7	2.17	5200	85	18	0.28	1.11E-03		...	b	...	5,6
13141	17848	A2V	5.3	50.7	1.88	8200	45	145	2.87	6.65E-05		100	a,d	MIPS	

Table 2—Continued

HIP	HD	Sp. Type	V (mag)	D (pc)	R_\star (R_\odot)	T_\star (K)	T_{dust} (K)	R_{dust} (AU)	angle (arcsec)	τ	Dust mass M_\oplus	age (Myr)	Age Method [†]	Dust Excess Confirmation	Notes ^α
(1)	(2)	(3)	(4)	(5)	(6)	(7)	(8)	(9)	(10)	(11)	(12)	(13)	(14)	(15)	(16)
14576	19356	B8V	2.1	28.5	4.13	9200	130	48	1.69	6.33E-06	2,6,7
15197	20320	A5m	4.8	36.8	2.00	7800	90	34	0.95	2.04E-05	2.59E-03	400?	a,d	MIPS	8
16449	21997	A3IV/V	6.4	73.8	1.57	9000	70	60	0.82	5.29E-04	1.92E-01 [‡]	50?	a,d	...	
16537	22049	K2V	3.7	3.2	0.69	5200	45	21	6.69	8.74E-05	2.32E-03 [‡]	730	S2000	MIPS/ISO	
18437	24966	A0V	6.9	103.5	1.50	10000	85	48	0.47	2.58E-04		10	d	...	
18859	25457	F5V	5.4	19.2	1.19	6400	80	17	0.92	1.25E-04	3.96E-03	30	a,b,c	MIPS/ISO	
18975	25570	F2V	5.4	36.0	1.83	7000	85	28	0.80	8.86E-05		600	Hyades	...	2
19704	27346	A9IV	7.0	114.5	2.57	7600	70	70	0.62	2.61E-04	1.40E-01	600?	a,d	...	2,9
19893	27290	F4III	4.3	20.3	1.65	7200	80	31	1.53	2.30E-05	2.42E-03	300?	a,b	...	10
20635	27934	A7IV-V	4.2	47.0	2.60	9000	85	67	1.44	4.72E-05	2.32E-02	600	Hyades	...	2
21010	28447	G5	6.5	39.7	2.05	5600	85	20	0.52	4.68E-04		2000??	a,b	...	11
21604	29365	B8V	5.8	110.7	3.06	8800	75	97	0.88	3.78E-04		200?	a,d	...	2,7
22226	30447	F3V	7.9	78.1	1.31	7200	65	37	0.48	9.47E-04	1.42E-01	\lesssim 100	a	MIPS	
22439	30743	F3/F5V	6.3	35.4	1.46	6400	40	86	2.45	2.28E-04	1.85E-01	>1000	a,b,c	...	2,12
22845	31295	A0V	4.6	37.0	1.67	9000	80	49	1.33	8.44E-05	2.22E-02	100?	a,d	MIPS	
23451	32297	A0	8.1	112.1	1.24	8400	85	28	0.25	5.38E-03	4.62E-01	20?	d	...	
24528	34324	A3V	6.8	85.8	1.59	8800	100	28	0.33	1.72E-04	1.48E-02	200?	d	...	
25197	34787	A0Vn	5.2	104.3	3.26	10000	120	52	0.50	6.97E-05	2.07E-02	400?	a,d	...	2
25790	36162	A3Vn	5.9	105.6	2.92	8800	85	72	0.69	2.49E-04		600?	a,d	...	13
26453	37484	F3V	7.2	59.5	1.36	7000	95	17	0.29	2.82E-04	8.94E-03	30	a,b,c	MIPS	
26966	38206	A0V	5.7	69.2	1.63	10000	90	46	0.68	1.67E-04	3.87E-02	50	a,d	MIPS	

Table 2—Continued

HIP	HD	Sp. Type	V (mag)	D (pc)	R_\star (R_\odot)	T_\star (K)	T_{dust} (K)	R_{dust} (AU)	angle (arcsec)	Dust mass	age (Myr)	Age Method [†]	Dust Excess	Confirmation	Notes ^α
(1)	(2)	(3)	(4)	(5)	(6)	(7)	(8)	(9)	(10)	τ	M_\oplus	(13)	(14)	(15)	(16)
27072	38393	F7V	3.6	9.0	1.18	6600	90	14	1.64	7.71E-06	4.48E-04 [‡]	>1000??	a,b	...	
27288	38678	A2Vann	3.5	21.5	1.65	9000	220	6	0.30	1.34E-04		100	a,d	MIPS	
27321	39060	A3V	3.9	19.3	1.37	8600	110	19	1.01	2.64E-03	8.99E-02 [‡]	12	β Pic	MIPS	
27980	39833	G0III	7.7	46.7	1.23	6000	70	20	0.45	2.79E-03		700	a,b,c	...	2,14
28230	40540	A8IVm	7.5	89.9	1.45	7800	90	25	0.28	6.06E-04		200	d	...	2,15
32480	48682	G0V	5.2	16.5	1.08	6400	130	6	0.37	2.16E-04		600??	a,b	...	16
32775	50571	F7III-IV	6.1	33.2	1.38	6600	45	68	2.08	1.63E-04	8.26E-02	300?	a,b,c	...	
33690	53143	K0IV-V	6.8	18.4	0.88	5400	60	16	0.90	1.88E-04	5.28E-03	300?	a,b,c	...	
34276	54341	A0V	6.5	92.9	1.59	10000	85	51	0.55	2.01E-04		10	d	...	17
34819	55052	F5IV	5.8	107.1	4.74	6800	45	251	2.35	1.01E-04		300??	a,c	...	2
35550	56986	F0IV...	3.5	18.0	2.13	7200	60	71	3.95	8.93E-06	4.94E-03	400??	a,b,d	MIPS	8
36906	60234	G0	7.6	108.6	2.78	6200	85	34	0.32	4.29E-04		600?	a,b	...	2
36948	61005	G3/G5V	8.2	34.5	0.81	5600	85	8	0.24	3.31E-03		100?	a,b,c	...	
39757	67523	F2mF5IIP	2.8	19.2	3.41	6800	85	50	2.64	5.38E-06		\gtrsim 2000	a,b,c	...	
40938	70298	F2	7.2	70.9	1.77	6800	85	26	0.37	3.54E-04		>3000	a,b	...	2
41152	70313	A3V	5.5	51.4	1.54	10000	80	56	1.09	5.24E-05	1.80E-02	200	a,d	MIPS	
41307	71155	A0V	3.9	38.3	2.02	10000	120	32	0.85	3.93E-05	4.41E-03	100	a,d	MIPS	
42028	72660	A1V	5.8	100.0	2.39	10000	85	77	0.77	7.07E-05		200	a,d	...	2
42430	73752	G3/G5V	5.1	19.9	1.73	5800	80	21	1.06	3.21E-05	1.55E-03	>600	S2000	...	18
42913	74956	A1V	1.9	24.4	3.90	9000	85	101	4.17	3.75E-06		400?	a,b,d	...	
43970	76543	A5III	5.2	49.0	1.86	8800	85	46	0.94	1.04E-04		400?	a,d	...	2

Table 2—Continued

HIP	HD	Sp.	Type	V	D	R_\star	T_\star	T_{dust}	R_{dust}	angle	τ	Dust mass	age	Age	Dust Excess	Confirmation	Notes ^α
				(mag)	(pc)	(R_\odot)	(K)	(K)	(AU)	(arcsec)		M_\oplus	(Myr)	Method [†]			
(1)	(2)	(3)	(4)	(5)	(6)	(7)	(8)	(9)	(10)	(11)	(12)	(13)	(14)	(15)	(16)		
44001	76582	F0IV	5.7	49.3	1.73	8000	85	35	0.72	2.22E-04		300??	a,d	...			
45758	80425	A5	6.6	98.1	2.43	7600	85	45	0.46	2.70E-04		300?	a,d	...	2		
48164	84870	A3	7.2	89.5	1.59	8000	85	32	0.37	5.48E-04		100	d	...	1		
48541	85672	A0	7.6	93.1	1.19	9200	85	32	0.35	4.82E-04		30?	a,d	...			
49641	87887	A0III	4.5	88.1	3.77	10000	90	108	1.23	4.89E-06		300?	a,d	MIPS			
51438	91375	A2III	4.7	79.4	3.10	10000	85	99	1.26	2.42E-05	2.60E-02	400??	a,d	...			
51658	91312	A7IV	4.7	34.3	1.84	8200	40	179	5.23	1.06E-04		200	a,d	...	8		
52462	92945	K1V	7.7	21.6	0.77	5200	45	23	1.11	6.74E-04	3.91E-02	100	SBZ	MIPS			
53524	95086	A8III	7.4	91.6	1.49	8200	85	32	0.35	1.49E-03		50	d	...	2,19		
53910	95418	A1V	2.3	24.3	2.84	10000	120	45	1.88	1.23E-05	2.73E-03	500	UMa	...			
53911	...	K8Ve	11.1	56.4	1.31	3600	140	2	0.04	>2.39E-01		8	TWHya	MIPS			
55505	98800	K4V	9.1	46.7	1.97	4200	160	3	0.07	1.12E-01		8	TWA	MIPS	8		
56253	99945	A2m	6.1	59.8	1.72	8200	85	37	0.62	1.04E-04		300?	a,d	...			
56675	101132	F1III	5.6	42.1	1.95	7000	50	88	2.11	1.42E-04		300	a,b,c,d	...	2		
57632	102647	A3Vvar	2.1	11.1	1.67	8800	160	11	1.06	4.25E-05	5.64E-04	50	S2001	MIPS			
57759	102902	G3V	7.4	87.7	3.15	5600	85	31	0.36	3.81E-04		>2000	a,b	...	2		
60074	107146	G2V	7.0	28.5	0.97	6200	60	24	0.85	1.08E-03	8.50E-02 [‡]	\lesssim 100	a,b,c	...			
61174	109085	F2V	4.3	18.2	1.62	6800	180	5	0.30	1.20E-04		300	a,b,c	MIPS			
61498	109573	A0V	5.8	67.1	1.59	10000	110	30	0.46	4.43E-03	2.11E-01 [‡]	8	HR 4796A	MIPS			
61782	110058	A0V	8.0	99.9	1.09	8800	130	11	0.12	2.54E-03	3.37E-02	10?	LCC	...	19,20		
61960	110411	A0V	4.9	36.9	1.49	9000	85	38	1.05	6.23E-05	9.86E-03	100??	a,d	MIPS			

Table 2—Continued

HIP	HD	Sp.	Type	V (mag)	D (pc)	R_\star (R_\odot)	T_\star (K)	T_{dust} (K)	R_{dust} (AU)	angle (arcsec)	τ	Dust mass M_\oplus	age (Myr)	Age Method [†]	Dust Excess Confirmation	Notes ^α
(1)	(2)	(3)	(4)	(5)	(6)	(7)	(8)	(9)	(10)	(11)	(12)	(13)	(14)	(15)	(16)	
63584	113337	F6V		6.0	37.4	1.50	7200	100	18	0.48	1.01E-04	3.59E-03	50?	a,b	...	21
64375	114576	A5V		6.5	112.6	2.63	8200	85	56	0.51	3.90E-04		600	a,d	...	1
64921	115116	A7V		7.1	85.4	1.53	8400	80	39	0.46	3.39E-04		100?	a,d	...	
68101	121384	G8V		6.0	38.1	2.95	5200	45	91	2.41	2.47E-04		>3000	a,b,c	...	
68593	122652	F8		7.2	37.2	1.07	6400	60	28	0.76	1.06E-04	9.11E-03	300?	a,b,c	MIPS	
69682	124718	G5V		8.9	61.3	0.98	5800	85	10	0.17	2.11E-03		>500	a,b,c	...	22
69732	125162	A0sh		4.2	29.8	1.72	9000	100	32	1.09	5.22E-05	5.86E-03	200?	a,d	MIPS	
70090	125473	A0IV		4.1	75.8	3.98	10000	120	64	0.85	2.11E-05	9.48E-03	300	a,d	...	
70344	126265	G2III		7.2	70.1	2.12	6200	85	26	0.37	3.85E-04		>500	a,b	...	
70952	127821	F4IV		6.1	31.7	1.30	6800	50	55	1.76	2.58E-04	8.26E-02 [‡]	200?	a,b	...	
71075	127762	A7IIIvar		3.0	26.1	3.08	8000	55	151	5.80	1.04E-05		1000	a,d	...	
71284	128167	F3Vwvar		4.5	15.5	1.39	6600	60	39	2.54	9.52E-06	6.37E-03 [‡]	1000??	a,b,c	ISO	
73049	131625	A0V		5.3	75.8	2.49	9000	85	64	0.86	7.39E-05		200	a,d	...	2
73145	131835	A2IV		7.9	111.1	1.26	8600	90	26	0.24	3.07E-03	2.28E-01	10	d	...	23
73473	132742	B9.5V		4.9	93.3	3.94	8800	150	31	0.34	7.22E-05	7.61E-03	500	a,d	...	2,7,24
73512	132950	K2		9.1	30.4	0.75	4800	85	5	0.18	1.17E-03		3000??	2
74596	135502	A2V		5.3	69.4	2.24	10000	65	123	1.77	3.26E-05		200	a,d	...	
74946	135382	A1V		2.9	56.0	5.86	9400	50	481	8.60	9.29E-06		700??	a,d	...	
75118	136407	F2V		6.1	54.6	2.20	6600	85	30	0.57	1.62E-04		600?	a,b	...	2
76127	138749	B6Vnn		4.2	95.3	4.16	10000	75	171	1.80	1.99E-05		200?	a,d	...	
76267	139006	A0V		2.2	22.9	2.72	10000	190	17	0.76	2.41E-05	7.64E-04	500	a,b,d	MIPS	7

Table 2—Continued

HIP	HD	Sp.	Type	V (mag)	D (pc)	R_\star (R_\odot)	T_\star (K)	T_{dust} (K)	R_{dust} (AU)	angle (arcsec)	τ	Dust mass M_\oplus	age (Myr)	Age Method [†]	Dust Excess Confirmation	Notes ^α
(1)	(2)	(3)	(4)	(5)	(6)	(7)	(8)	(9)	(10)	(11)	(12)	(13)	(14)	(15)	(16)	
76375	139323	K3V		7.6	22.3	0.85	5200	40	33	1.51	5.40E-04		5000??	a,b	...	2,25
76635	139590	G0V		7.5	55.1	1.40	6200	85	17	0.31	3.93E-04		5000??	a,b	...	
76736	138965	A5V		6.4	77.3	1.47	9600	130	18	0.24	1.23E-04		20	a,d	MIPS	2
76829	139664	F5IV-V		4.6	17.5	1.26	7000	75	25	1.46	1.15E-04	7.88E-03	200?	a,b,c	MIPS	
77163	140775	A1V		5.6	117.8	3.25	10000	40	472	4.01	1.39E-04		600	a,d	...	26
77542	141569	B9		7.1	99.0	1.49	9200	110	24	0.25	1.12E-02	3.32E-01 [‡]	5	HD 141569	...	
77811	142096	B3V		5.0	109.3	3.90	9400	110	66	0.61	3.50E-04	1.67E-01	200?	a,d	...	
78554	143894	A3V		4.8	54.3	2.27	9000	45	211	3.89	4.64E-05		300	a,d	...	
81126	149630	B9Vvar		4.2	92.7	4.91	9400	80	157	1.70	3.01E-05		700	a,d	...	1
81641	150378	A1V		5.8	92.9	2.23	10000	95	57	0.62	1.24E-04	4.42E-02	200	a,d	...	1
81800	151044	F8V		6.5	29.4	1.21	6200	55	35	1.22	8.30E-05	1.11E-02	>500	a,b	MIPS/ISO	
82405	151900	F1III-IV		6.3	59.8	2.30	6600	85	32	0.54	2.98E-04		>1000	a,d	...	2
83137	153377	F2		7.5	61.1	1.30	6800	85	19	0.32	7.38E-04		>600	a,b	...	2
83480	154145	A2		6.7	94.9	1.99	8400	85	45	0.48	4.28E-04		300?	d	...	26
85157	157728	F0IV		5.7	42.8	1.43	8600	90	30	0.71	2.67E-04	2.63E-02	100?	a,d	...	
85537	158352	A8V		5.4	63.1	2.52	8400	110	34	0.54	1.66E-04	2.10E-02	600?	a,d	...	
87108	161868	A0V		3.7	29.1	1.91	9400	85	54	1.87	7.84E-05	2.51E-02	200?	a,d	MIPS	
87558	162917	F4IV-V		5.8	31.4	1.50	6600	85	20	0.67	2.49E-04		400?	a,b,c	...	
88399	164249	F5V		7.0	46.9	1.27	6800	70	27	0.60	1.03E-03	8.23E-02	12	ZSBW	MIPS/ISO	
90185	169022	B9.5III		1.8	44.3	6.66	10000	100	155	3.50	4.46E-06		300??	a,b,d	...	
90936	170773	F5V		6.2	36.1	1.34	7000	50	61	1.69	4.16E-04	1.70E-01	200?	a,b,c	ISO	

Table 2—Continued

HIP	HD	Sp. Type	V (mag)	D (pc)	R_\star (R_\odot)	T_\star (K)	T_{dust} (K)	R_{dust} (AU)	angle (arcsec)	τ	Dust mass M_\oplus	age (Myr)	Age Method [†]	Dust Excess Confirmation	Notes ^α
(1)	(2)	(3)	(4)	(5)	(6)	(7)	(8)	(9)	(10)	(11)	(12)	(13)	(14)	(15)	(16)
91262	172167	A0Vvar	0.0	7.8	2.58	10000	80	93	12.10	2.14E-05	8.37E-03 [‡]	220	Vega	...	
92024	172555	A7V	4.8	29.2	1.52	8000	320	2	0.08	8.10E-04		12	ZSBW	MIPS	
93542	176638	A0Vn	4.7	56.3	2.11	10000	120	34	0.60	9.70E-05	1.23E-02	200?	a,d	...	
95261	181296	A0Vn	5.0	47.7	1.61	9600	120	23	0.50	2.40E-04	1.39E-02	12	ZSBW	MIPS/ISO	
95270	181327	F5/F6V	7.0	50.6	1.39	6600	75	25	0.50	3.47E-03	2.38E-01	12	ZSBW	MIPS	
95619	182681	B8/B9V	5.7	69.1	1.71	10000	85	55	0.80	1.95E-04		50?	a,d	...	
96468	184930	B5III	4.3	94.3	4.01	10000	60	259	2.75	3.52E-05		2,6
98025	189207	F2	8.1	118.3	1.74	7400	85	30	0.26	7.41E-04		100?	a,b	...	2
99273	191089	F5V	7.2	53.5	1.39	6600	95	15	0.29	1.39E-03	3.43E-02	\lesssim 30	a,b,c	MIPS	8
99473	191692	B9.5III	3.2	88.0	6.63	10000	85	213	2.43	6.60E-06		500?	a,d	...	
101612	195627	F1III	4.8	27.6	1.70	7400	65	51	1.86	1.11E-04	3.17E-02	200?	a,d	MIPS	
101769	196524	F5IV	3.6	29.9	3.63	6800	130	23	0.77	1.56E-05	9.05E-04	200??	a,b,c	...	2,8
101800	196544	A2V	5.4	54.3	1.65	9000	100	31	0.57	3.86E-05	4.07E-03	30	a,d	MIPS	8
102409	197481	M1Ve	8.8	9.9	0.86	3500	50	9	0.98	3.64E-04	8.80E-03 [‡]	12	ZSBW	MIPS	
103752	199475	A2V	6.4	83.3	1.83	8800	85	45	0.55	2.45E-04		200	a,d	...	2
104206	199391	F0/F2IV	7.1	84.8	1.66	7800	80	36	0.43	2.48E-04		>600	b	...	1,2
105570	203562	A3V	5.2	110.4	4.02	9000	85	104	0.95	8.80E-05		600?	a,d	...	1
106741	205674	F3/F5IV	7.2	52.6	1.22	7200	85	20	0.39	3.96E-04		300?	a,b	...	
107022	205536	G8V	7.1	22.1	0.89	5600	80	10	0.46	2.92E-04	3.20E-03	>500	a,b	...	
107412	206893	F5V	6.7	38.9	1.24	6600	55	41	1.07	2.72E-04	3.18E-02 [‡]	200?	a,b	MIPS/ISO	
107649	207129	G2V	5.6	15.6	0.98	6000	55	27	1.74	1.21E-04	9.67E-03	600	SZB	ISO	

Table 2—Continued

HIP	HD	Sp. Type	V (mag)	D (pc)	R_\star (R_\odot)	T_\star (K)	T_{dust} (K)	R_{dust} (AU)	angle (arcsec)	τ	Dust mass M_\oplus	age (Myr)	Age Method [†]	Dust Excess Confirmation	Notes ^α
(1)	(2)	(3)	(4)	(5)	(6)	(7)	(8)	(9)	(10)	(11)	(12)	(13)	(14)	(15)	(16)
108809	209253	F6/F7V	6.6	30.1	1.10	6200	80	15	0.51	1.52E-04	3.75E-03	200??	a,b,c	ISO	
109857	211336	F0IV	4.2	25.7	1.86	7800	65	62	2.41	1.56E-04	6.58E-02	600?	a,c,d	...	
110867	210681	K0III	8.1	61.8	1.87	5200	85	16	0.26	7.15E-04	2,6
113368	216956	A3V	1.2	7.7	1.81	8600	65	73	9.60	7.98E-05	2.41E-02 [‡]	220	Fomalhaut	...	
114189	218396	A5V	6.0	39.9	1.37	7800	50	77	1.94	2.29E-04	1.00E-01 [‡]	30	a,d	ISO	
116431	221853	F0	7.3	71.2	1.48	7400	85	26	0.37	7.38E-04	5.47E-02	≤100	a	MIPS/ISO	

Note. — Calculations use 1 AU=215 R_\odot

[†]Age Methods: S2000: Song et al. (2000); S2001: Song (2001); SBZ: Song et al. (2002a); ZFK: Zuckerman et al. (1995b); ZSBW: Zuckerman et al. (2001a); ZSW: Zuckerman et al. (2001b); ZW: Zuckerman & Webb (2000); SZB: Song, Zuckerman, & Bessell (2003); a: UVW ; (Zuckerman & Song 2004b); b: X-ray emission; e.g., Song, Zuckerman, & Bessell (2003); c: lithium age; (Song, Zuckerman, & Bessell 2003); d: location on an A-star Hertzsprung-Russell diagram; (Lowrance et al. 2000)

[‡]Dust mass measurements are directly from submillimeter observations.

^α 1. binary.

2. New debris disk candidate.
3. HIP 7345 (=49 Cet) is the only known main sequence A-type star with CO emission detected with a radio telescope (ZFK), thus suggesting a very young age. But its galactic space motion UVW ($-23, -17, -4$) with respect to Sun is not indicative of extreme youth (U is positive toward the Galactic center).
4. HIP 8241 shows the age of the Pleiades on an A star HR diagram (Lowrance et al. 2000) but of the Hyades in UVW measurements.
5. There is a galaxy at $\sim 48''$ East of HIP 13005 in cross-scan direction as described in Paper I. However, a more careful check of the IRAS 60 μm offset using the FSC long format indicates that both IRAS 12 μm and 60 μm detections have the same offsets away from the galaxy in the same cross-scan direction. Thus, we include HIP 13005 with a caution.
6. No age estimate is given for HIP 13005, HIP 14576, HIP 96468, & HIP 110867
7. Eclipsing binary of the Algol type.
8. Spectroscopic binary.
9. There are two FSC detections for HIP 19704 separated by $34''$. One has 12 and 25 μm detections, the other has a 60 μm detection. The long format of FSC locates the 60 μm source on HIP 19704.
10. In addition to the point-like 60 μm source reported in the FSC, there is an extended optical source $70''$ from the IRAS position of HIP 19893 in the in-scan

Table 3. Algols from IRAS and *Spitzer*

HIP	HD	Other	Rieke et al. (2005)		This Paper		Triple System?
			Observed?	Excess?	Excess?		
14576	19356	Algol A	yes	1.07 (no)	marginal?	yes	
21604	29365	HU Tau	no		strong	?	
28360	40183	β Aur	yes	0.88 (no)	nothing	?	
73473	132742	δ Lib	no		2 wavelengths	yes	
76267	139006	α CrB	yes	1.29 (yes)	2 wavelengths	?	